Edinburgh Research Explorer

Drag Reduction and Leidenfrost Effect on Submerged Ratcheted Cylinder

Drag Reduction and Leidenfrost Effect on Submerged Ratcheted Cylinder

Adrian Jonas, Daniel Orejon & Khellil Sefiane

Published online: 17 Jan 2023.

Submit your article to this journal ↗

Article views: 193

View related articles ↗

View Crossmark data ↗

Taylor & Francis
Taylor & Francis Group

OPEN ACCESS

Check for updates

Drag Reduction and Leidenfrost Effect on Submerged Ratcheted Cylinder

Adrian Jonas (iD), Daniel Orejon (iD), and Khellil Sefiane (iD)

Institute for Multiscale Thermofluids, School of Engineering, University of Edinburgh, Edinburgh, UK

ABSTRACT

This paper presents experimental investigations of submerged self-propulsion due to the Leidenfrost effect. We aim to identify and quantify the forces governing the free-fall of heated cylinders at temperatures between 25 °C and 550 °C. Understanding the forces involved within three-phase systems is essential when designing sensitive instruments, such as microelectronic devices. Cylinders with sizes in the range of tens of millimeters are released into a vertical column filled with Novec 7000. Experiments were conducted to investigate five topological designs, and bored-out hollows within the cylinders forced vertical free-fall. The control cylinder was smooth, while the others had ratchet teeth engraved on their surface. Ratcheted cylinders were manufactured in pairs to compare ratchet directionality. An in-house tracking tool reduced experimental error and measurement noise. The time taken to reach terminal velocity increases with initial temperature while terminal velocity decreases, respectively. The depth at which terminal velocity occurs also decreases with increasing initial temperature. The existence of submerged self-propulsion has been identified by comparing ratcheted cylinders of opposing directionality. A theoretical mechanism for the action of the viscous friction force that drives self-propulsion has been developed. The viscous friction force has been quantified to be between 0.04–3.28 mN.

Introduction

In 1756, Johann Gottlob Leidenfrost [1] extensively studied the levitation of droplets on hot surfaces. Since dubbed the Leidenfrost effect, the levitation of droplets is a case of thin-film boiling whereby a water droplet levitates on its own evaporate. The same effect is observed for different liquids boiling within the Leidenfrost regime [2,3]. Solids undergoing sublimation [4,5] also demonstrate similar behavior. The motion of these levitating liquid droplets and solid components is virtually frictionless. If heated on a smooth base, the evaporate or sublimate is expelled symmetrically [6], where an asymmetry in the expelled vapor flow will lead to a low-friction self-propulsion of the liquid droplet [7,8], or the sublimating solid [9]. Linke et al. [7] were the first to demonstrate that liquid droplets could propel themselves on ratcheted surfaces when heated above the Leidenfrost point. Several underlying mechanisms have since been proposed for Leidenfrost self-propulsion, including Marangoni flows [10], jet thrust [4], drag force due to thermal creep induced flows [11], and drag force due to vapor rectification [7,12]. Figure

1 shows self-propulsion based on viscous friction, which is the most widely studied mechanism and has been used to explain both the motion of solids and liquids [13]. Numerical [14] and analytical models [9] corroborated with experimental observations [15] show that the asymmetry of a substrate rectifies the vapor flow exiting in a specific direction. Self-propulsion of evaporating liquids and sublimating solids occurs then on various textured substrates such as ratchets [16], herringbones [12], and asymmetric microstructures [17]. The Leidenfrost effect, which converts thermal energy to mechanical or electrical energy, can, in turn, be transferred to translate [15,18,19] or rotate [20] nonvolatile objects. The torque transfer from the active substance to solid components provides the basis for developing a mechanical heat engine using the Leidenfrost effect. Wells et al. [20] demonstrated dry ice rotation on turbine-like substrates[20], and subsequently, sustained rotation of droplets has produced net torque [13].

Beyond droplets, supercavitation has also attracted relevant interest. Supercavitation is when a liquid changes phase into vapor due to a significant decrease in

Nomenclature

2.2FD	Ratcheted cylinder with the flat side of the ratchets facing downward during free-fall and a ratchet aspect ratio (h/w) defined by 2.2, where $h = 1.1$ mm and $w = 0.5$ mm		L	Length of a cylinder, measured from the base of the cylinder to the base of the cone surmounted at the leading end, m
2.2FU	Ratcheted cylinder with the flat side of the ratchets facing upward during free-fall and a ratchet aspect ratio (h/w) defined by 2.2, where $h = 1.1$ mm and $w = 0.5$ mm		l	Depth of the hollow within a free-falling cylinder, m
			m	Mass, kg
			P	Pitch of the surmounted cone, or height of the cone, m
11.4FD	Ratcheted cylinder with the flat side of the ratchets facing downward during free-fall and a ratchet aspect ratio (h/w) defined by 11.4, where $h = 5.7$ mm and $w = 0.5$ mm		Pl	Path length of free-falling cylinder, m
			px	Pixels covering the width of the cylinder
			py	Pixels covering the length of the cylinder
			SC	Smooth cylinder
11.4FU	Ratcheted cylinder with the flat side of the ratchets facing downward during free-fall and a ratchet aspect ratio (h/w) defined by 11.4, where $h = 5.7$ mm and $w = 0.5$ mm		s	Depth measured when a free-falling cylinder reached terminal velocity, m
			t	Time, s
			v	Velocity, m/s
AR	Aspect ratio		V	Volume, m³
D	Diameter of a smooth cylinder, excluding the length added by the ratchet widths, m		w	Ratchet width or perpendicular length concerning the cylinder length of the engraved ratchets, m
d	Diameter of the hollow within a free-falling cylinder, m		x	Distance associated with the width of the column, m
F	Force, N		y	Distance associated with the length of the column, m
FD	Downward facing ratchets, where the face of a ratchet is its flat side concerning a ratcheted cylinder			
fps	Frames per second		**Greek Symbols**	
FU	Upward facing ratchets, where the face of a ratchet is its flat side concerning a ratcheted cylinder		β	Pixel/distance ratio
			ρ	Density, kg/m³
g	Gravity, m/s²		σ	Absolute error
HSC	High-speed camera		**Subscripts**	
h	Ratchet height or parallel length concerning the cylinder length of the engraved ratchets, m		B	Buoyancy
			c	Cylinder
$IH25$	An unheated cylinder, defined as the isothermal condition, whereby the room temperature was recorded at $23 \pm 3\,°C$, in so far as both the bulk fluid and cylinder are assumed at equal temperature		D	Drag
			f	Fluid
			G	Gravity
			i	Associated with the subject of interest
			Pl	Path length
			R	Resultant
$IH50$	A cylinder that is initially heated to $50\,°C$		RC	Ratcheted cylinder
$IH150$	A cylinder that is initially heated to $150\,°C$		SC	Smooth cylinder
$IH250$	A cylinder that is initially heated to $250\,°C$		t	Terminal velocity
$IH350$	A cylinder that is initially heated to $350\,°C$		VF	Associated with the viscous friction force
$IH450$	A cylinder that is initially heated to $450\,°C$		x	Distance associated with the width of the column
$IH550$	A cylinder that is initially heated to $550\,°C$		y	Distance associated with the length of the column

pressure. When fluid flows over a bluff body in a stream, the fluid flow over the body's surface increases in velocity, and under the right conditions, conservation of energy reduces the flow pressure surrounding the body to cause the phase change. The resulting three-phase system almost eliminates skin friction drag causing submerged bodies to achieve extremely high speeds [21–24]. In 1977, the Soviet Navy introduced the Shkval torpedo, a supercavitating weapon that traveled through a body of water at more than 100 m/s [25]. More recently, Vakarelski *et al.* [26] showed that at lower speeds, the Leidenfrost effect also shows drag-reducing characteristics for superheated spheres, suggesting the increased turbulence within the vapor layer delays flow separation of the wake, resulting in a smaller drag coefficient. Combining a continuous and lubricating vapor layer with the self-propelling nature of ratchets could prove to change the way we think about drag reduction. Rather than view the drag reduction problem as simply reducing either; the flow separation, or the surface area in contact with the fluid [27] – we propose that drag may be reduced by rectifying flow around an object in the direction of motion. Figure 1 shows that when a droplet boils atop a solid surface in the Leidenfrost regime, the fluid is levitated above the surface with evaporated fluid expulsion. This expulsion of vapor can be directed with asymmetric shapes such as ratchets to produce microflows that drive the droplet. The direction of motion follows the direction of vapor flow, where it is speculated that the propelling mechanism is that of viscous drag. We aim to exploit the propulsion mechanism to increase the speed of traveling objects immersed in a fluid and decrease drag.
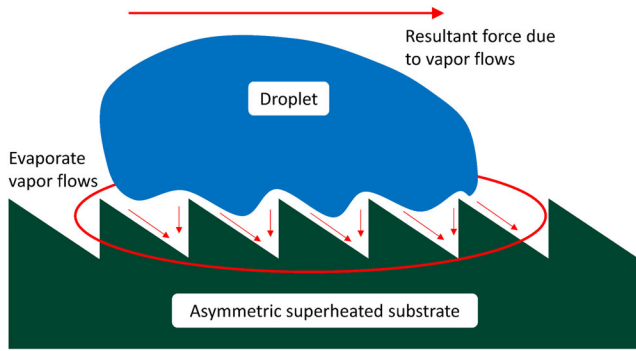
Figure 1. A schematic showing the self-propelling physical mechanism of a Leidenfrost droplet atop a superheated substrate. Microflows beneath the droplet generate a viscous drag force which moves the droplet to the right.

Experimental

Cylinder samples

The relevant dimensions for the cylinders used in this investigation are found in Table 1. Cylinders are defined as; Control – which indicates that the topology at the mm scale is smooth, FU – which indicates that the flat side of the ratchets engraved onto the cylinder are facing upwards, and FD – which indicates that the flat side of the ratchets engraved onto the cylinder are facing downwards. Notice in Table 1 that two aspect ratios (2.2 and 11.4) were investigated. We define the aspect ratio in equation (1).

$$AR = h/w \tag{1}$$

Where AR is the aspect ratio, h is the length of the ratchet parallel to the length of the cylinder, and w is the perpendicular length. Lagubeau et al. [4] reported the self-propelling viscous drag force to be in the order of μN. Therefore, ratchets engraved along the length of the cylinders would maximize the chances of observing self-propulsion. Unfortunately, Chu et al. [28] found that free-falling uniform cylinders tend to orientate themselves horizontally; however, they reported that one could force a cylinder to fall vertically by separating the center of mass from the center of volume. Given the range of temperatures our experiments occur at, we chose to hollow the cylinders out.

Table 1. Dimensions of cylinder design used within this experimental investigation.

Description

Label	Ratchet direction	D (mm)	d (mm)	L (mm)	l (mm)	P (mm)	h (mm)	w (mm)	h/w
Control	–	10	8.5	40	27	3	N/A	0	N/A
FD 2.2	Down	10	8.5	40	27	3	1.1	0.5	2.2
FU 2.2	Up	10	8.5	40	27	3	1.1	0.5	2.2
FD 11.4	Down	10	8.5	40	27	3	5.7	0.5	11.4
FU 11.4	Up	10	8.5	40	27	3	5.7	0.5	11.4

D: cylinder diameter (±0.3 mm), d: hollow diameter (±0.3 mm), L: cylinder length (±0.3 mm), l: hollow depth (±0.3 mm), P: pitch height (±0.3 mm), h: ratchet height, w: ratchet width.

Table 2. Relevant heat transfer properties for substances used within these experiments.

Description	Density (kg/m³)	Boiling/Melting Point (°C)	Viscosity (cSt)	Latent Heat (kJ/kg)	Specific Heat Capacity (J/kg K)	Thermal Conductivity (W/m K)
Aluminum (s)	2700	660	–	–	900	225
Novec7000 (l)	1400	34	0.32	142	1300	0.075

Properties are given at ambient temperature and ambient pressure.
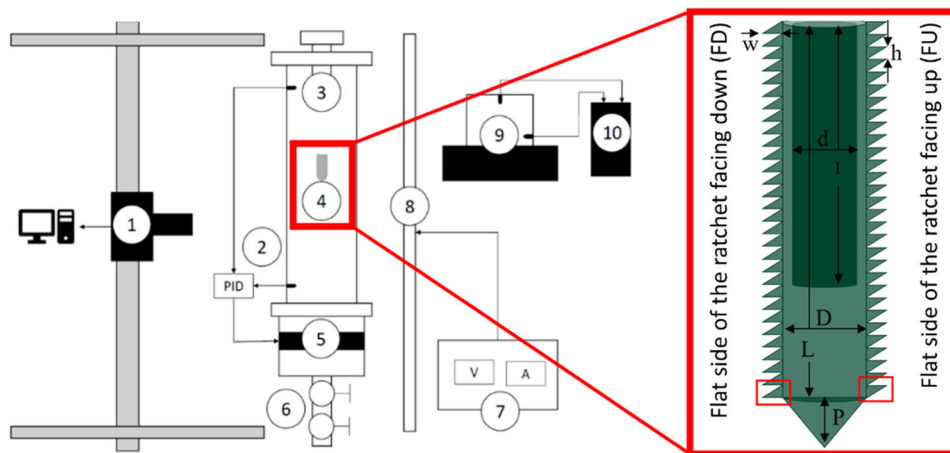

Figure 2. Experimental Schematic. (1) Chronos 2.1 HSC. (2) Temperature Control. (3) Guiding Release Shoot. (4) Cylinder. (5) Heater. (6) Extraction Unit. (7) Power Supply. (8) Strip Light. (9) Oven. (10) Controller.
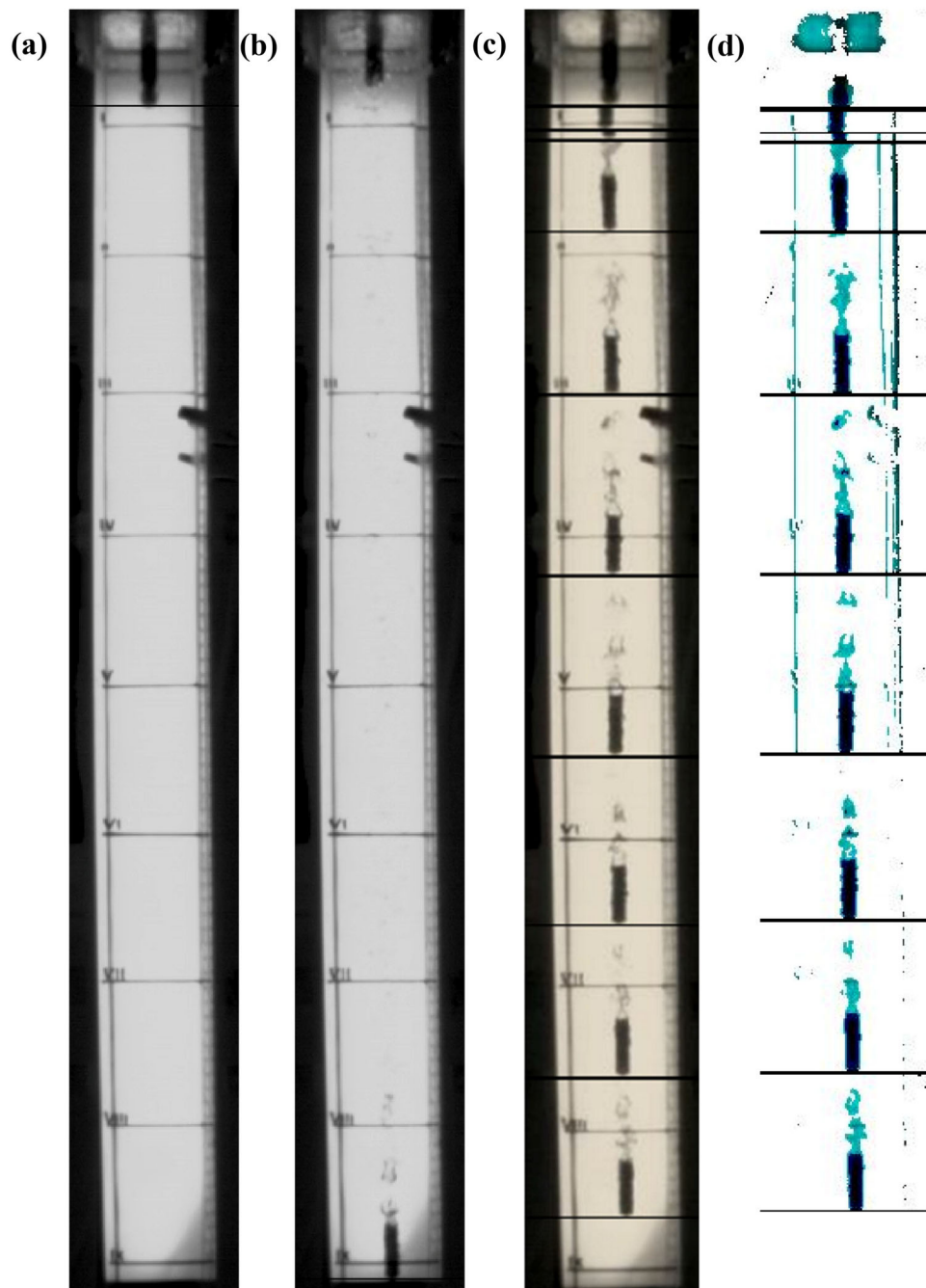
Figure 3. Initial frame (a), final frame (b), trajectory (c), and processed trajectory (d) for a smooth cylinder heated to 550 °C.

Analyzing the drag forces on either side of the center of gravity gave us the confidence that a cylinder with a hollow 62.5% of its length and 85% of its diameter (Table 1) will cause it to fall vertically. In hollowing the cylinders, we also reduce the energy any given cylinder can store. To maximize the probability of achieving the Leidenfrost effect then, we chose aluminum which has a significantly high specific heat capacity among common metals. Table 2 summarizes the density and thermal properties of both aluminum and Novec 7000 at ambient pressure and ambient temperature. Manufacturing ratchets into aluminum cylinders at this scale is technically challenging, resulting in

imperfect ratchet structures, especially for ratchets with an aspect ratio of 2.2, i.e., FD 2.2 and FU 2.2.

Experimental setup

A detailed schematic of the experimental setup and a sketch of the ratcheted cylinders can be found in Figure 2. We use an extruded acrylic square tube to hold approximately 9 liters (1500 mm × 70.45 mm × 70.45 mm) of Novec 7000 (1-methoxyheptafluoropropane). The bottom end of the column is held in place

with an aluminum flange that attaches to a steel extraction unit. The extraction unit funnels matter into a central extraction tube. The extraction tube contains two inline ball valves to remove cylinders from the column without losing Novec 7000. Naturally, the loss of Novec 7000 is unavoidable using this method, so excess Novec 7000 from the extraction tube is collected and poured back into the column. Losses of Novec 7000 are restored to the standard level with more after each experiment. Novec 7000 remains at room temperature throughout the experiments (Table 2), recorded as $23 \pm 3\,°C$. At the upper end, the column is sealed with a flange containing two inlets. The first is for the release of cylinders used in the experiments, the second is a pressure relief measure, and to aid with the release of superheated cylinders. For experiments involving cylinders above the boiling point of the pool, we found that a 'chimney thrust' would prevent the full submersion of cylinders before falling freely. Thus, we employ a guiding release shoot to ensure true free-fall occurred only once the cylinders were submerged. The release shoot consisted of large venting holes allowing the escape of vapor out into the column. Our experiments consisted of heating cylinders in an electric oven (Efco Enameling Kiln 180 KF) positioned next to the column to $50\,°C$, $150\,°C$, $250\,°C$, $350\,°C$, $450\,°C$, and $550\,°C$ before removing them by hand and releasing them to fall into the column. Given aluminum's melting point of $\sim600\,°C$, our experimental temperature maximum was $550\,°C$ as to avoid unintentional tampering of the ratchet structures. The electric oven was controlled by a PID (Efco Temperature Controller TRP008 – Digital) and used a thermocouple to monitor the temperature. The experimental runs were defined by the temperature at which the oven was set. A high-speed camera (HSC) 2.1 – Chronos HD was used to capture the fall of released cylinders within the column. The HSC was held in place with a rail mechanism that allowed movement forwards and backwards and upwards and downwards. Our presented results will primarily consider the information at steady state (terminal velocity). Preliminary experiments showed that terminal velocity, across all temperatures, occurs at a depth of $\sim0.5\,m$. Therefore, we set the center of image capture at a depth of $\sim0.5\,m$ (Figure 3). All experiments were captured at a framerate of 1000 frames-per-second (fps). A wide-angle lens was employed to capture as much of the cylinders' fall as possible, forcing a maximum resolution of 1920×100 pixels. This resolution could capture $1.5\,m$ of fall, though our experiments were limited by the

1 m length of strip light we had available. The strip light was positioned behind the column to provide a contrast sufficient for image processing.

Experimental procedures

First the column was sealed, and the HSC settings were calibrated to accommodate the light conditions of the day. The position of the HSC was not altered throughout the acquisition of these experimental results. Five iterations for a given initial temperature were conducted in a row. Cylinders were released in order of topography. (i.e., Smooth, 2.2FD, 2.2FU, 11.4FD, 11.4FU). For the isothermal experiment, the experiments were done in the morning giving time for the temperature of the cylinders and pool to equilibrate. Once the camera had been set, a smooth cylinder was released into the column. The footage was immediately saved and cataloged. Then, using the extraction valves at the bottom of the column the cylinder was removed and the column fluid level was restored. The camera was set to record again and so the 2.2FD cylinder was released into the pool. The process described above was repeated for all the cylinders. The experimental runs were repeated five times for each cylinder for each temperature setting. For the
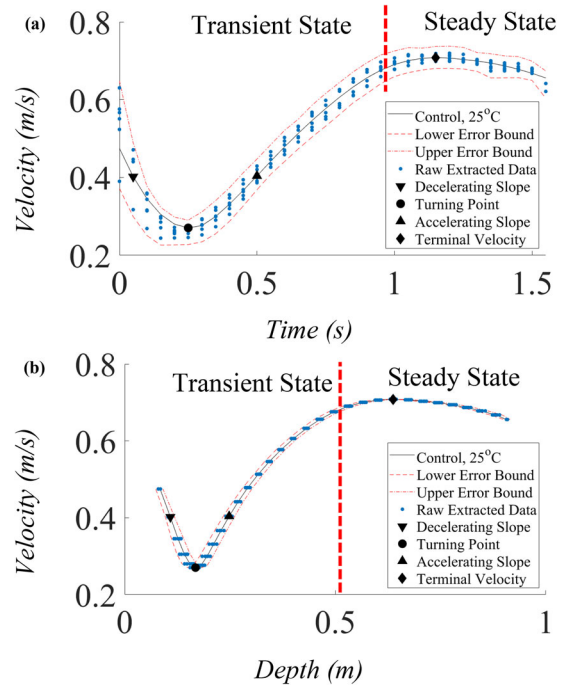

Figure 4. Errors are graphically represented for the random error in velocity v (m/s) versus time t (s) (a) and in velocity v (m/s) versus depth (b) for a smooth cylinder falling in isothermal conditions. Vertical red dashed lines are included as an approximation to characterize the fall into two states of free-fall: transient state; and steady state.

heated experiments, the cylinders were first inspected and placed in order within the oven. The oven was then allowed to equilibrate at its set temperature and was to maintain that temperature for 15 minutes before experiments began. To release the cylinders into the pool, a single cylinder was removed from the oven with tweezers and placed into the guiding release shoot to fall freely into the column. The column was immediately sealed once the cylinder was released as not to lose Novec 7000. The camera was then stopped, footage catalogued, cylinder removed, and column filled to the standard level. This step was again repeated for each cylinder, five times over.

Measurement methods

K-type thermocouples, calibrated using a standard laboratory thermometer, were used to monitor the temperature of the pool. The temperature of the cylinder was assumed to be the temperature the oven was set at, and it could not be measured as it moved through the fluid. Depth was controlled and measured using markings drawn of the face of the column. The markings were drawn using a standard meter rule. For each experiment the level of the pool was returned to zero by toping up any loss of Novec 7000.

Methodology

Existing software which could process the HSC footage led to significant errors and experimental noise. Therefore, we made use of a bespoke software tool (Moxie Analyzer) that can find a moving object within a video, track its position, and calculate physical parameters such as velocity and acceleration. Figure 3 shows the initial (Figure 3(a)) and final (Figure 3(b)) frames used to calibrate the Moxie Analyzer for a free-falling smooth cylinder heated to 550 °C. The Moxie Analyzer requires the experimentalist to insert spatial measurements used as calibration points to convert pixels to distance values. The frame rate defines the experiment's time acquisition, and important physical parameters are calculated with distance-time relations. A HSC decreases the time between each data acquisition, increasing the accuracy of the calculated parameters. The tracking tool also produces a processed image (Figure 3(d)) from the original captured footage (Figure 3(c)), which shows the experimentalist the free-fall trajectory and provisional vapor layer thickness. The noise reduction procedure of the data produced by the tracking tool is displayed. Raw data overlapped by data produced

from a robust quadratic regression algorithm built within MATLAB removes noise from the results. Points extracted at equal intervals of time are plotted in Figure 4 and shows the output of the noise reduction algorithm. Experimental iterations identify random errors. presents the extracted data from 5 iterations at isothermal conditions and their corresponding errors. Figure 4(a) shows errors in velocity across experimental iterations, while Figure 4(b) shows errors in depth. The time error comes from the frame rate used to capture the data. Preliminary experiments determined that at terminal velocity, film boiling occurs for cylinders initially heated to temperatures to 350 °C and beyond, nucleate boiling occurs for cylinders initially heated to temperatures to 150 °C and beyond, and single-phase free-fall is observed for cylinders initially heated to 50 °C and below.

Data reduction

The Moxie Analyzer software requires an image of the column with only liquid Novec 7000 present which it finds from the first image in a video uploaded to it, named the mask. The subsequent images are then subtracted from the mask, giving a value between 255 and 0 for every pixel within an image. A value near 0 would indicate that no object was present and a value larger than 150 would indicate certainty. The Moxie Analyzer checks every associated pixel value from the bottom of the column to the top, and the moment the Moxie Analyzer registers a value between 65 and 90 it marks the frame and pixel at which the object was located. A value between 65 and 90 is used to guarantee that the point marked is the leading edge of the cylinder. The Moxie analyzer presents the experimentalist with the initial and final frames from which frame and pixel data was stored. Here, the experimentalist inputs the real-time depth and estimated error seen from the markings drawn on the face of the column. These readings give the Moxie Analyzer a pixel/distance value (β) which it uses to determine position. The Pythagorean theorem described in equation (2) was used to calculate path length.

$$Pl = \frac{\sqrt{py^2 + px^2}}{\beta} \qquad (2)$$

Where Pl is path length, β is the pixel/distance ratio, px is the pixels covering the width of the column, and py is the pixels cover the length of the column. Time is allocated with the framerate used to capture images, which was consistently set to 1000
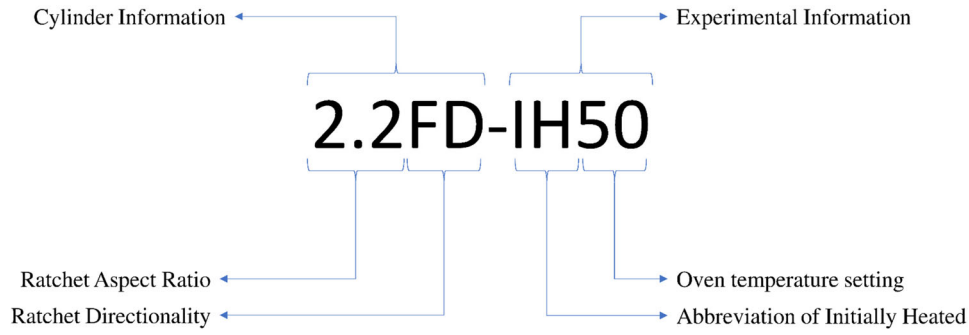
Figure 5. Symbology used to describe experimental information within the body of the text.
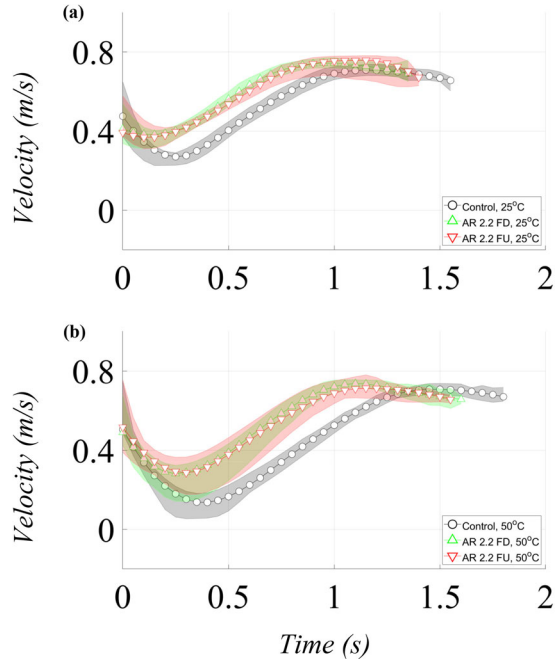

Figure 6. Single-phase experimental results for control and ratcheted cylinders with ARs of 2.2 with an initial temperature of 25 °C (a) and at 50 °C (b) falling through a column filled with Novec 7000 at room temperature.

fps. Equation (3) show that the velocity of the cylinder is then calculated using the central difference method.

$$v = \frac{(Pl_{i+1}) - (Pl_{i-1})}{(t_{i+1} - t_{i-1})} \qquad (3)$$

Where v is velocity, Pl_i is the spatial distance relative to the first point recorded, t_i is the time elapsed since the first frame calculated using the framerate of capture. A built-in MATLAB function named "*smooth*" was then used to remove noise from the data. MATLAB describes the function as "*A robust local regression using weighted linear least squares and a 2nd degree polynomial model which assigns lower weight to outliers in the regression. The method assigns zero weight to data outside six mean absolute deviations.*" From this regressed data, representative points of time, depth, and velocity, were extracted at intervals of 0.05 s defined again by the framerate.

Uncertainty

The first element of uncertainty came from the measurement of depth made with the initial and final frames presented by the Moxie Analyzer, which was defined as ±0.005 m in most cases. Given two measurements, the absolute error for calibration was 0.01 m. The typical distance covered by measurements was 0.83 m giving a typical relative uncertainty of 1%. The camera captures images at a 1000 ± 0.005 fps. A typical experiment lasted 2 seconds, and therefore a typical experiment used 2000 frames. The relative error associated with time is then negligible, but we report temporal measurement errors at 0.00005%, i.e., the relative error associated with image capture. Using the calculated relative errors in measurement, we calculate an absolute error in space (x, y) and time (t) for each frame where the cylinder was observed. To calculate the errors associated to the path length of the cylinders free-fall, we applied the "propagation of errors" formula described in equation (4).

$$\sigma_{Pl} = \left(\frac{dPl}{dx}\right)_y^2 \sigma_x^2 + \left(\frac{dPl}{dy}\right)_x^2 \sigma_y^2 \qquad (4)$$

Where σ_{Pl} is the absolute error in pathlength, $\frac{dPl}{dx}$ is the magnitude of pathlength associated with a change in x-position, σ_x is the absolute error associated with the change in x-position, $\frac{dPl}{dy}$ is the magnitude of pathlength associated with a change in y-position, σ_y is the absolute error associated with the change in y-position. The relative error associated with path length and time was then calculated, which was used to calculate the relative error associated with each calculated velocity value. A regression was preformed using the data captured from five experimental iterations. After calculating the absolute velocity errors, the residual errors taken from the regression were added. Five repeated experiments help identify the random errors, giving an area of uncertainty around the regression lines.
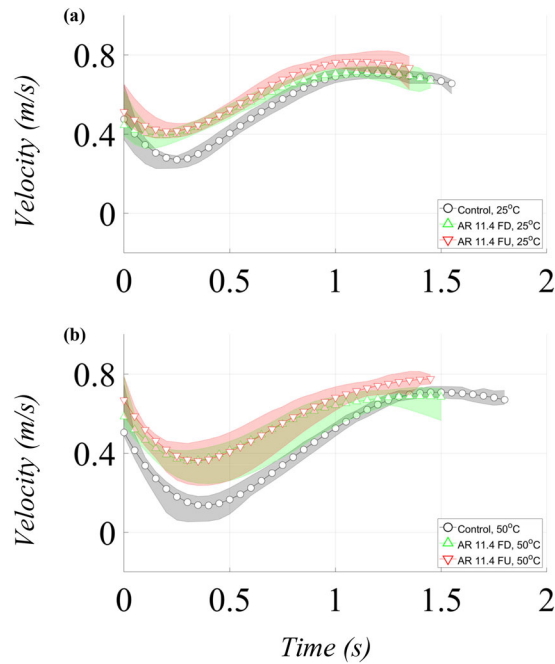
Figure 7. Single-phase experimental results for control and ratcheted cylinders with aspect ratios of 11.4 with an initial temperature of 25 °C (a) and at 50 °C (b) falling through a column filled with Novec 7000 at room temperature.

Results

Here we present our results in boiling regime and ratchet aspect ratio (AR) categories. Control runs are duplicated across ARs within all figures presented herein. The trajectory of a free-falling cylinder can be simplified into two states, the transient-state, and steady-state. The transient state is defined by an initial deceleration after an impact with the pool's surface, to then reach a turning point where the cylinder begins to accelerate again which is followed by an acceleration. The plateau that follows the acceleration is what we define as the start of the steady-state condition, as represented in Figure 4. Figure 5 shows the symbology used to simplify the categorization of the experiments within this paper.

Single-phase

Experimental runs at 25 °C represent isothermal conditions. Though the boiling point of Novec 7000 is 36 °C, cylinders initially heated to 50 °C present as single-phase experiments following an analysis of the high-speed footage captured, where little to no vapor was observed within the steady state condition. These observations imply that cylinders initially heated to 50 °C would cool to below 36 °C before reaching terminal velocity. Experimental runs using a smooth control cylinder and ratcheted cylinders defined by an
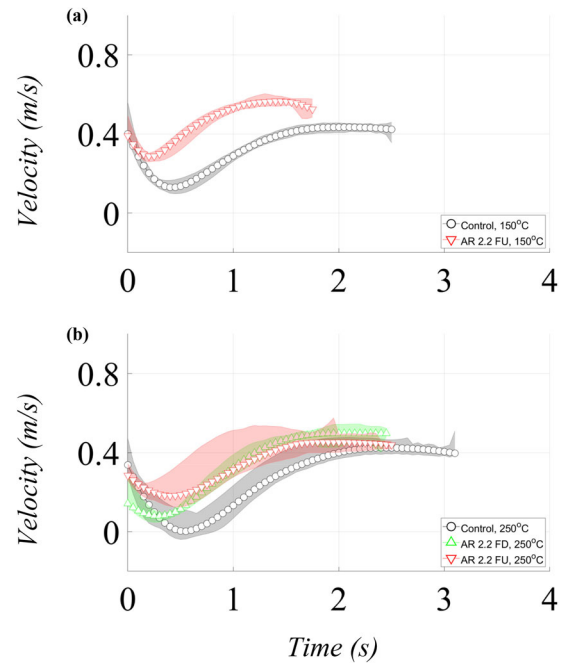

Figure 8. Nucleate boiling experimental results for control and ratcheted cylinders with aspect ratios of 2.2 with an initial temperature of 150 °C (a) and at 250 °C, (b) falling through a column filled with Novec 7000 at room temperature. At 150 °C, disturbances associated with imploding and coalescing bubbles prevented a single successful run to be completed with the FD cylinder.

AR of 2.2 at 25 °C and 50 °C are presented in Figure 6.

Control

A smooth cylinder falling at isothermal conditions (SC-IH25) is initially observed to decelerate at -1.30 m/s^2 for 0.25 s. The cylinder starts to accelerate with an initial velocity of 0.27 ± 0.03 m/s, increasing at a rate of 0.75 m/s^2. For a smooth cylinder initially heated to 50 °C (SC-IH50), the cylinder decelerates at -1.68 m/s^2 for 0.40 s to a velocity of 0.14 ± 0.07 m/s. SC-IH50 then accelerates at 0.80 m/s^2.

Aspect ratio 2.2

For ratcheted cylinders with an AR of 2.2, we observe cylinders that fall with greater velocities. An initial inspection does not show a considerable directional dependence. Consider the cylinder with the flat side of the ratchets facing downwards. At isothermal conditions, the cylinder (2.2FD-IH25) slows at a rate of -0.26 m/s^2 for 0.15 s to a velocity of 0.38 ± 0.05 m/s before accelerating at 0.76 m/s^2. Comparatively, the same cylinder initially heated to 50 °C (2.2FD-IH50) decelerates at -1.31 m/s^2 for 0.25 s. The initial velocity follows at 0.28 ± 0.09 m/s and increases at a rate of

$0.47\,\text{m/s}^2$. Again, if we consider a cylinder falling at isothermal conditions with the flat side of the ratchet facing upwards (2.2FU-IH25), we observe an initial deceleration of $-0.24\,\text{m/s}^2$ for $0.10\,\text{s}$ to a velocity of $0.37 \pm 0.07\,\text{m/s}$. The cylinder then accelerates at $0.67\,\text{m/s}^2$. The same cylinder, now initially heated to $50\,^{\circ}\text{C}$ (2.2FU-IH50), will initially decelerate at $-1.28\,\text{m/s}^2$ to a velocity of $0.27 \pm 0.10\,\text{m/s}$. After $0.30\,\text{s}$, the cylinder will accelerate at $0.73\,\text{m/s}^2$ toward its terminal velocity after reaching the initial velocity.

Aspect ratio 11.4

A ratcheted cylinder defined by an AR of 11.4 at $25\,^{\circ}\text{C}$ and $50\,^{\circ}\text{C}$ is compared against the smooth control in Figure 7. Cylinders falling within a single phase carrying this ratcheted topology also fall faster than their smooth counterparts regardless of the ratchet directionality. A cylinder at isothermal conditions, defined by an AR of 11.4, and a ratchet directionality in line with the fall – downwards (11.4FD-IH25) will decelerate at $-0.39\,\text{m/s}^2$ to reach an initial velocity of $0.39 \pm 0.04\,\text{m/s}$ after $0.20\,\text{s}$ before accelerating at $0.53\,\text{m/s}^2$. The same cylinder heated to $50\,^{\circ}\text{C}$ (11.4FD-IH50) will decelerate at $-1.17\,\text{m/s}^2$ to $0.36 \pm 0.08\,\text{m/s}$. $0.30\,\text{s}$ into the fall, the 11.4FD-IH50 cylinder accelerates at $0.54\,\text{m/s}^2$. When a cylinder defined by an AR of 11.4 and ratchets that face upwards falls at isothermal conditions (11.4FU-IH25), the cylinder will initially decelerate at
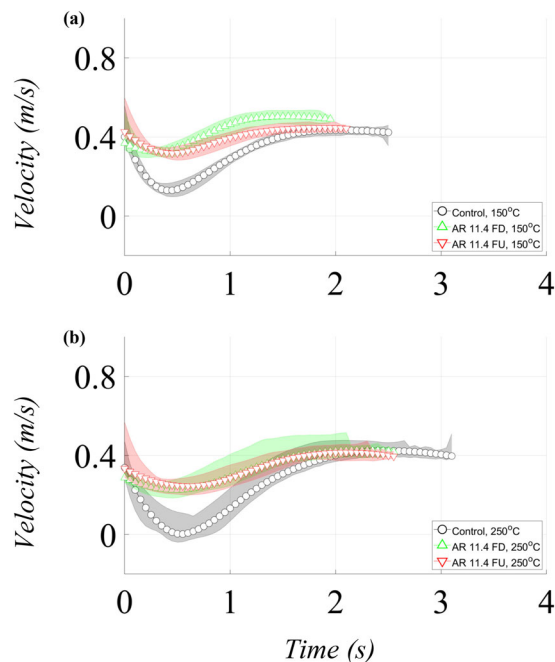
$-0.69\,\text{m/s}^2$ to $0.41 \pm 0.04\,\text{m/s}$ after $0.20\,\text{s}$, before accelerating at $0.64\,\text{m/s}^2$ to reach steady-state. This time initially heated to $50\,^{\circ}\text{C}$ (11.4FU-IH50); the velocity of the cylinder initially reduces at a rate of $-1.49\,\text{m/s}^2$ breaking the pool's surface to a velocity of $0.36 \pm 0.11\,\text{m/s}$. It takes $0.35\,\text{s}$ before a cylinder begins to accelerate to its terminal velocity at a rate of $0.62\,\text{m/s}^2$.

Nucleate boiling

Experiments within the nucleate boiling regime, i.e., temperatures between $150\,^{\circ}\text{C}$ and $250\,^{\circ}\text{C}$, are presented in Figures 8 and 9. A further visual inspection determined the nucleate boiling regime of the experiments. The nucleate boiling regime presents a highly unstable free-fall, so much in fact that for the cylinder with upward-facing ratchets defined by an AR of 2.2, and initially heated to $150\,^{\circ}\text{C}$ (2.2FD-IH150), no experiments within the constraints of our setup were able to complete the fall without touching the walls of the column.

Control

The trajectory of the same smooth cylinder, used in the single-phase experiments, but this time initially heated to $150\,^{\circ}\text{C}$ (SC-IH150), begins to fall down the

Figure 9. Nucleate boiling experimental results for control and ratcheted cylinders with aspect ratios of 11.4 with an initial temperature of $150\,^{\circ}\text{C}$ (a) and at $250\,^{\circ}\text{C}$ (b) falling through a column filled with Novec 7000 at room temperature.

Figure 10. Film boiling experimental results for control and ratcheted cylinders with aspect ratios of 2.2 with an initial temperature of $350\,^{\circ}\text{C}$ (a), $450\,^{\circ}\text{C}$ (b), and at $550\,^{\circ}\text{C}$ (c) falling through a column filled with Novec 7000 at room temperature.
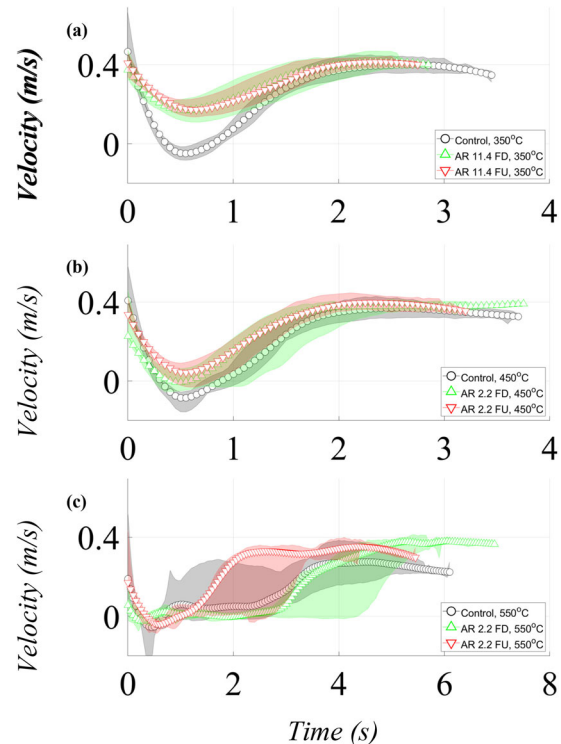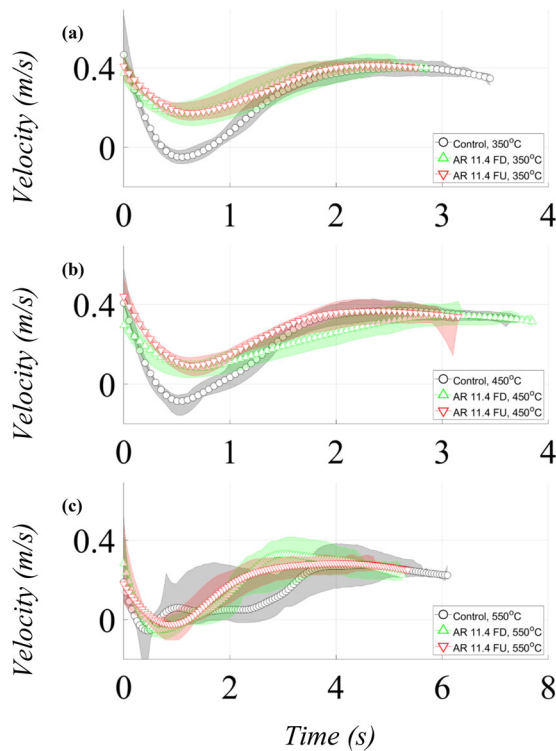
Figure 11. Film boiling experimental results for control and ratcheted cylinders with aspect ratios of 11.4 with an initial temperature of 350 °C (a), 450 °C (b), and at 550 °C (c) falling through a column filled with Novec 7000 at room temperature.

column with a deceleration of $-1.15 \, \text{m/s}^2$. The deceleration lasts 0.40 s before accelerating from $0.13 \pm 0.03 \, \text{m/s}$ at a rate of $0.34 \, \text{m/s}^2$. Comparatively, the same cylinder initially heated to 250 °C (SC-IH250) will decelerate to $0.00 \pm 0.07 \, \text{m/s}$ at a rate of $-1.13 \, \text{m/s}^2$ for 0.55 s before accelerating at $0.42 \, \text{m/s}^2$.

Aspect ratio 2.2

Figure 8 shows the results for the cylinders defined by an AR of 2.2 and the control sample results. The ratcheted cylinder used in the single-phase experiments, defined by an AR of 2.2 and ratchets that face downwards, is initially heated to 250 °C (2.2FD-IH250). The cylinder is first slowed by $-0.36 \, \text{m/s}^2$ for 0.3 s to a velocity of $0.08 \pm 0.03 \, \text{m/s}$. The following acceleration presents at $0.44 \, \text{m/s}^2$. Similarly, the cylinder defined again by an AR of 2.2, with ratchets that face the trailing end, is initially heated to 150 °C (2.2FU-IH150). The cylinder will initially decelerate at $-0.72 \, \text{m/s}^2$ for 0.20 s to a velocity of $0.29 \pm 0.02 \, \text{m/s}$ leading to an acceleration of $0.45 \, \text{m/s}^2$. The same cylinder but heated to 250 °C (2.2FU-IH250) presents a trajectory that follows a deceleration of $-0.43 \, \text{m/s}^2$ for 0.40 s. The resulting velocity of $0.18 \pm 0.09 \, \text{m/s}$ comes before an acceleration at a rate of $0.30 \, \text{m/s}^2$ to its terminal velocity.

Aspect ratio 11.4

Figure 9 presents the investigations of AR 11.4 along with the results on the control sample. Like experiments run within the single-phase regime, ratcheted cylinders fall with a greater velocity. The deceleration of the cylinder defined by downward facing ratchets at an AR of 11.4 is initially heated to 150 °C (11.4FD-IH150). The cylinder slows by $-0.24 \, \text{m/s}^2$ for 0.30 s to a velocity of $0.33 \pm 0.03 \, \text{m/s}$. The cylinder then begins to accelerate at $0.26 \, \text{m/s}^2$ toward its terminal velocity. The same cylinder heated to 250 °C (11.4FD-IH250) will slow by $-0.23 \, \text{m/s}^2$ for 0.50 s to a velocity of $0.23 \pm 0.06 \, \text{m/s}$. The cylinder then accelerates at $0.21 \, \text{m/s}^2$. The counterpart, a cylinder with upwards facing ratchets defined by an AR of 11.4 when initially heated to 150 °C (11.4FU-IH150), follows a deceleration of $-0.42 \, \text{m/s}^2$ for 0.45 s. After reaching a velocity of $0.32 \pm 0.03 \, \text{m/s}$, the cylinder increases at a rate of $0.18 \, \text{m/s}^2$. That same cylinder heated to 250 °C (11.4FU-IH250) initially slows by $-0.27 \, \text{m/s}^2$ for 0.60 s. Then accelerates from $0.25 \pm 0.04 \, \text{m/s}$ to its terminal velocity at a rate of $0.19 \, \text{m/s}^2$.

Film boiling

Film boiling presents increased uncertainty though more stable free-falls occur as compared against the nucleate boiling regime. We observe a significantly different trajectory from the nucleate boiling and single-phase experiments within the film boiling regime. A smooth cylinder can be seen to reverse its motion toward the pool's surface, cooling before descending toward the bottom. This trend is also observed when using ratcheted cylinders but less consistently. After breaking the pool's surface, the reverse in motion for a smooth control cylinder occurs after being initially heated to 250 °C, 350 °C, 450 °C, and 550 °C.

In contrast, only three ratcheted cylinders achieve negative velocities after being initially heated to 550 °C, while the cylinder with downward-facing ratchets defined by an AR of 2.2 will reverse its motion after being initially heated to 450 °C and

Table 3. Summary of the initial decelerations (m/s^2) for the different cylinders (Control, 2.2FD, 2.2FU, 11.4FD, and 11.4FU) and temperatures (including the single-phase, nucleate boiling and film boiling regimes).

Descriptions	Single-phase		Nucleate boiling			Film boiling	
	IH25	IH50	IH150	IH250	IH350	IH450	IH550
Control	−1.3	−1.68	−1.15	−1.13	−1.76	−1.68	−0.98
2.2FD	−0.26	−1.31	x	−0.36	−1.12	−0.85	−0.5
2.2FU	−0.24	−1.28	−0.72	−0.43	−0.6	−0.96	−0.64
11.4FD	−0.39	−1.17	−0.24	−0.23	−0.7	−0.56	−0.91
11.4FU	−0.69	−1.49	−0.42	−0.27	−0.67	−0.97	−0.43

Table 4. Summary of the deceleration periods (s) for the different cylinders (Control, 2.2FD, 2.2FU, 11.4FD, and 11.4FU) and temperatures (including the single-phase, nucleate boiling and film boiling regimes).

	Single-phase		Nucleate boiling			Film boiling	
Descriptions	IH25	IH50	IH150	IH250	IH350	IH450	IH550
Control	0.25	0.4	0.4	0.55	0.8	0.88	0.68
2.2FD	0.15	0.25	x	0.3	0.4	0.58	2.15
2.2FU	0.1	0.3	0.2	0.4	0.5	0.55	0.97
11.4FD	0.2	0.3	0.3	0.5	0.55	0.7	1.23
11.4FU	0.2	0.35	0.45	0.6	0.65	0.65	1.23

Table 5. Summary of the initial velocities (m/s) for the different cylinders (Control, 2.2FD, 2.2FU, 11.4FD, and 11.4FU) and temperatures (including the single-phase, nucleate boiling and film boiling regimes).

	Single-phase		Nucleate boiling			Film boiling	
Descriptions	IH25	IH50	IH150	IH250	IH350	IH450	IH550
Control	0.27	0.14	0.13	0	0	0	0
2.2FD	0.38	0.28	x	0.08	0.07	0	0
2.2FU	0.37	0.27	0.29	0.18	0.15	0.04	0
11.4FD	0.39	0.36	0.33	0.23	0.17	0.08	0
11.4FU	0.41	0.36	0.32	0.25	0.17	0.09	0

Table 6. Summary of the acceleration (m/s^2) toward terminal velocity, v_t, for the different cylinders (Control, 2.2FD, 2.2FU, 11.4FD, and 11.4FU) and temperatures (including the single-phase, nucleate boiling and film boiling regimes).

	Single-phase		Nucleate boiling			Film boiling	
Descriptions	IH25	IH50	IH150	IH250	IH350	IH450	IH550
Control	0.75	0.8	0.34	0.42	0.47	0.46	0.26
2.2FD	0.76	0.47	x	0.44	0.41	0.45	0.37
2.2FU	0.67	0.73	1.4	0.3	0.35	0.36	0.37
11.4FD	0.53	0.54	0.26	0.21	0.24	0.17	0.25
11.4FU	0.64	0.62	0.18	0.19	0.23	0.28	0.24

550 °C. These trends within the film boiling regime, i.e., temperatures between 350 °C and 550 °C, are presented in Figures 10 and 11. Again, ARs have been separated, with Figure 10 presenting control and AR 2.2 and Figure 11 including control and AR 11.4.

Control

For a smooth cylinder initially heated to 350 °C (SC-IH350), 450 °C (SC-IH450), and 550 °C (SC-IH550), acceleration begins from a stationary position after 0.80 s, 0.88 s, and 0.68 s respectively. These control experiments decelerate at $-1.76\,m/s^2$, $-1.68\,m/s^2$, and $-0.98\,m/s^2$ before accelerating at $0.47\,m/s^2$, $0.46\,m/s^2$, and $0.26\,m/s^2$.

Aspect ratio 2.2

Only the downward-facing ratcheted cylinder, defined by an AR of 2.2, initially heated to 450 °C (2.2FD-IH450), and 550 °C (2.2FD-IH550), along with an upward-facing ratcheted cylinder, defined again by an AR of 2.2, and initially heated to 550 °C (2.2FU-IH550)

present to reverse their motion back toward the surface of the pool. These experiments accelerate from stationary after 0.58 s, 2.15 s, and 0.97 s, respectively. Furthermore, these experiments initially decelerate at $-0.85\,m/s^2$, $-0.50\,m/s^2$, and $-0.64\,m/s^2$ before accelerating toward their terminal velocities at $0.45\,m/s^2$, $0.37\,m/s^2$, and $0.37\,m/s^2$, respectively. Experiments with the downward-facing and upward-facing ratcheted cylinders, defined by an AR of 2.2, were initially heated to 350 °C (2.2FD-IH350 and 2.2FU-IH350) and 450 °C (2.2FU-IH450) resulted in typical trajectories seen within the single-phase and nucleate boiling regimes. The initial decelerations of $-1.12\,m/s^2$, $-0.60\,m/s^2$, and $-0.96\,m/s^2$, which last for 0.40 s, 0.50 s, and 0.55 s, and result with initial velocities of $0.07 \pm 0.02\,m/s$, $0.15 \pm 0.06\,m/s$, and $0.04 \pm 0.06\,m/s$. The trajectories accelerate toward their respective terminal velocities at $0.41\,m/s^2$, $0.35\,m/s^2$, and $0.36\,m/s^2$.

Aspect ratio 11.4

Figure 11 shows the results for the cylinders defined by an AR of 11.4, contrasted by the smooth control results. Here, both cylinders defined by an AR of 11.4, which have opposing ratchet directionality, are heated to 550 °C (11.4FD-IH550 and 11.4FU-IH550) decelerate at $-0.91\,m/s^2$ and $-0.43\,m/s^2$. They both move upwards for 1.23 s after initially becoming submerged and accelerate toward their terminal velocity from a stationary position at a rate of $0.25\,m/s^2$ and $0.24\,m/s^2$. All other experiments using ratcheted cylinders defined by an AR of 11.4 fall with a similar trajectory to seem with the single-phase and nucleate boiling regimes. The downward-facing ratcheted cylinder, initially heated to 350 °C (11.4FD-IH350), decelerates at $-0.70\,m/s^2$ for 0.55 s, after which the cylinder accelerates to the terminal velocity from $0.17 \pm 0.06\,m/s$ at a rate of $0.24\,m/s^2$. The same cylinder heated to 450 °C (11.4FD-IH450) instead decelerates at $-0.56\,m/s^2$ for 0.70 s to a velocity of $0.08 \pm 0.04\,m/s$, where an acceleration of $0.17\,m/s^2$ follows. For the cylinder with upward-facing ratchets, here initially heated to 350 °C (11.4FU-IH350), a deceleration for 0.65 s at $-0.67\,m/s^2$ occurs. The result is a velocity of $0.17 \pm 0.05\,m/s$ before accelerating at $0.23\,m/s^2$ toward its terminal velocity. That same cylinder, now heated to 450 °C (11.4FU-IH450), decelerates at $-0.97\,m/s^2$ for 0.65 s before accelerating from a velocity of $0.09 \pm 0.05\,m/s$ at $0.28\,m/s^2$.

A summary of the initial deceleration can be found in Table 3. Table 4 summarizes the deceleration period, while a summary of the initial velocity can be found in Table 5. Table 6 presents the different
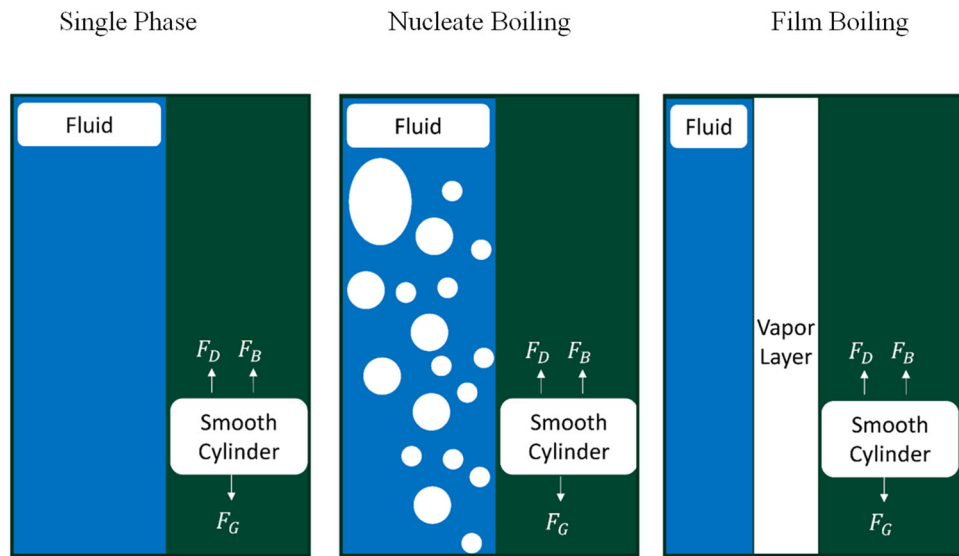
Single Phase   Nucleate Boiling   Film Boiling

Figure 12. Force analysis for a free-falling smooth cylinder in the; single phase, nucleate boiling, and film boiling regimes. Interfacial forces between three phases are assumed negligible, leaving a balance of gravitational forces, buoyancy forces, and drag forces. Differences in observed velocity are believed to be associated with changes in the buoyancy and drag forces around a smooth cylinder.
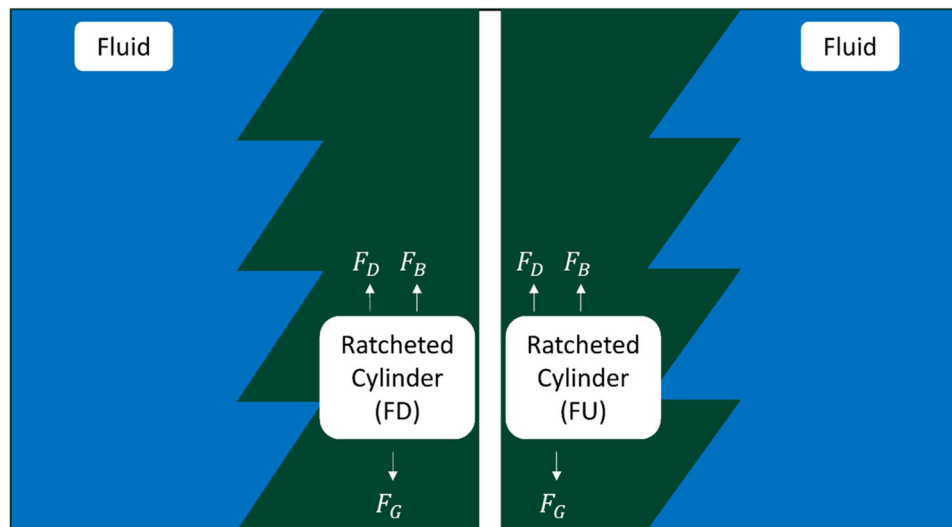

Figure 13. Force analysis for free-falling ratcheted cylinders in the single-phase boiling regime. There is no vapor and therefore the traditional methods of representing interfacial forces between two phases are used, in so far as they are fully represented by the drag coefficient. Here, a balance of gravitational, buoyancy, and drag forces describe the fall characteristics.

cylinders' acceleration values toward terminal velocity, v_t. Tables 3 and 4 include data for each cylinder (Control, 2.2FD, 2.2FU, 11.4FD, and 11.4FU) at each of the seven temperatures (including the single-phase, nucleate boiling, and film boiling regimes).

Analysis

The general behavior of a submerged free-falling cylinder begins with a plunge that breaks a pool's surface. An expected parabolic increase in velocity over time is observed to a terminal velocity designated as the steady-state condition. A summary of this behavior,

first described in the preceding section, can be found in Table 3–6. Any additional forces are assumed to be associated with viscous drag originating from the flow of vapor over the surface of the moving cylinder [7].

Physical mechanisms and governing forces

The basic understanding of submerged free-fall involves forces of gravity, buoyancy and drag. Figure 12 depicts this in the case of a smooth cylinder. We say that for a smooth cylinder, viscous friction forces are negligible. Any influence of vapor on the system is represented within the change in buoyancy force or
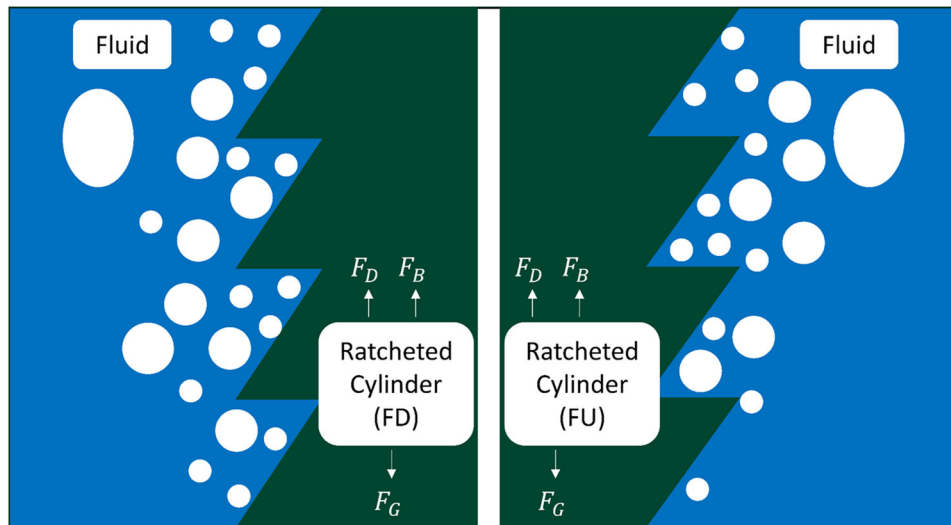
Figure 14. Force analysis for free-falling ratcheted cylinders in the nucleate boiling regime. A vapor film is not fully developed and therefore a more complex understanding of interfacial forces cannot be developed. Here we continue to rely on the traditional framework of a balance between gravitational, buoyancy, and drag forces.
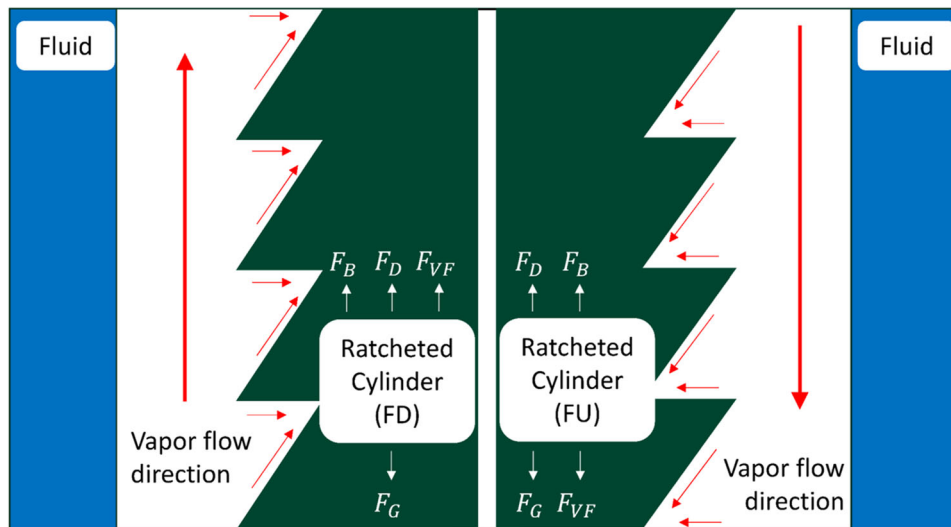

Figure 15. Force analysis for free falling ratcheted cylinders in the film boiling regime. A more complex understanding of interfacial forces can be developed. Here we include the viscous friction force (F_{VF}) which acts in relation to ratchet directionality. Vapor flow is rectified by the ratchets giving a resultant force parallel to the position of the cylinder, either upwards or downwards.

the change in drag force. In the case of a boiling object falling faster compared to the same object falling within the single phase, the situation is simple. One can assume that the buoyancy for the boiling object is unaffected by the vapor, which allows you to calculate a drag force and subsequent drag coefficient. For cases where the boiling object reduces in velocity, such as ours, the situation is complicated. Here, it is not clear whether an increase in drag or an increase in buoyancy is the cause for the reduction in velocity.

Figure 13 shows a similar argument for ratcheted cylinders falling within the single phase. The influence of ratchet directionality will simply be absorbed by

adopting an alternative drag coefficient. Figure 14 shows ratcheted cylinders falling within the nucleate boiling regime. Again, the situation follows tradition by using the drag force or buoyancy force to explain the change in behavior.

Figure 15 shows ratcheted cylinders falling within the film boiling regime. Here, the viscous friction force becomes a significant factor. Our hypothesis predicts that asymmetric shapes, such as ratchets, on the surface of the cylinder will either increase the resultant force pulling the cylinder deeper into the pool when the flat side of the ratchets are facing upwards (FU) or increase the force working against gravity

when the flat side of the ratchets are facing downwards (FD).

The structure of our analysis will first address the transient state, defined within Figure 4, for each of the five cylinders used at each of the seven temperatures. At this stage, we will only introduce the transient state as a supplement to our arguments, as this paper focuses on the behavior of cylinders at their steady state. It is essential to know the general behavior of cylinders on their journey to steady state, as these insights can help explain some of the trends seen for cylinders at their terminal velocity.

For example, consider the comparison between 2.2FD-IH550 and 2.2FU-IH550. When only considering the steady-state we see that 2.2FD-IH550 ($v_t = 0.37 \pm 0.06$ m/s) falls faster than 2.2FU-IH550 ($v_t = 0.33 \pm 0.18$ m/s). This result could easily be interpreted as – *"ratchet self-propulsion drives submerged substrates, where viscous drag forces slow upward-facing ratcheted cylinders more than their downward-facing counterparts."*; however, if we consider the transient state of this result, we see that 2.2FD-IH550 takes 2.15 s to begin accelerating to its terminal velocity compared to 0.97 s for 2.2FU-IH550 (Table 3). This extended fall time associated with the transient state will cause the 2.2FD-IH550 cylinder to cool down to a lower temperature than 2.2FU-IH550. Thus, when the cylinders accelerate toward their respective terminal velocity, 2.2FD-IH550 will be colder than 2.2FU-IH550. We then also notice that both experiments yield the same acceleration toward terminal velocity (0.37 m/s^2), and both cylinders begin their acceleration from a stationary point. So, assuming gravity remains constant and acts equally on both cylinders, one can balance the forces associated with vapor buoyancy, skin friction, form drag, and viscous self-propulsion. Knowing that 2.2FD-IH550 is colder than 2.2FU-IH550, the former cylinder will have a thinner vapor layer as it accelerates toward and reaches terminal velocity. The thinner vapor occurs because of the reduced temperature difference between the bulk fluid and the respective cylinder. Therefore, 2.2FD-IH550 should experience a smaller buoyancy force associated with the surrounding vapor when compared to 2.2FU-IH550. We also expect 2.2FD-IH550 to experience a viscous self-propelling force in the direction of the fall, and we expect 2.2FU-IH550 to experience a viscous self-propelling force to act in the opposite direction. So before even considering how a thicker vapor layer affects skin friction and/or form drag – our initial conclusion is uncertain. If we assume form drag and skin friction to be constant in both cases – the question concerning these two cases now becomes; *"Are our observations due to a reduction in vapor volume, or ratchet directionality?"*

Here, the reader is encouraged to apply the line of reasoning above to every reported terminal velocity value, as what is initially a conclusive result becomes unclear and uncertain when considering what happened on the journey before.

Transient-state

As earlier illustrated in Figure 4, the transient state consists of a cylinder being nominally slowed by the impact, then stabilizing to gain velocity under the pull of gravity once again. The impact following the release of cylinders into the pool causes instability, creating a transition state whereby the inertia gained prior to submersion is corrected. Next, we address the effect of temperature and hence boiling regime on the transient state, i.e., the period before the cylinder reaches almost terminal velocity v_t.

Single phase

Generally, isothermal cylinders decelerate less rapidly than cylinders initially heated to 50 °C after the initial impact, with a mean difference across all topologies of 0.81 m/s^2. Isothermal cylinders will also tend to slow down to a higher velocity than cylinders initially heated to 50 °C, differing by 0.08 m/s on average. Intuitively then, isothermal cylinders average less time (0.14 s) than their hotter counterparts decelerating. Interestingly, how a cylinder accelerates changes by introducing surface topologies with millimeter and submillimeter range features. For the cylinder, 2.2FU-IH50, the result shows accelerations greater than its isothermal counterpart by 0.06 m/s^2. The same is true for SC-IH25, which accelerates 0.05 m/s^2 faster than SC-IH50. This does not hold for the 11.4FD-IH25 experiment, which accelerates 0.01 m/s^2 faster than 11.4FD-IH50. Conversely, the 2.2FD-IH50 experiment will accelerate less than the 2.2FD-IH25 by 0.29 m/s^2, and experiment 11.4FU-IH50 will accelerate 0.02 m/s^2 faster than experiment 11.4FU-IH25.

Nucleate boiling

For cylinders in the nucleate boiling regime, we notice the opposite initial trend to that observed for single-phase free-fall. Generally, the hotter cylinder (250 °C) decelerates less rapidly than the cooler cylinder (150 °C) by 0.12 m/s^2 after averaging across all topologies. A cylinder initially heated to 150 °C takes an

average of 0.18 s less time decelerating than a cylinder initially heated to 250 °C. Also, cylinders initially heated to 150 °C will accelerate at a greater average velocity of 0.10 m/s compared to cylinders initially heated to 250 °C. Like the single-phase regime, the acceleration is affected by surface topology. The SC-IH150 and 11.4FU-IH150 experiments accelerate at 0.08 m/s² and 0.01 m/s² lower rates than their SC-IH250 and 11.4FU-IH250 counterparts. For cylinders 2.2FU-IH250 and 11.4FD-IH250, we see greater accelerations than their 2.2FU-IH150 and 11.4FD-IH150 counterparts, differing by 1.10 m/s² and 0.05 m/s², respectively. 2.2FD-IH150 could not be compared due to the instabilities seen.

Film boiling

For a smooth topology, the higher the initial temperature, the lesser the decelerating force after impact; however, this does not indicate a trend regarding the length of time a cylinder is cooling before descending the column downwards. The acceleration toward terminal velocity appears to decrease with temperature, indicating a more significant vapor volume presence and influence. An AR of 2.2 also presents smaller decelerating forces as temperatures increase, but only for cylinders with downward-facing ratchets. There seems to be no apparent trend concerning acceleration magnitudes; however, the time taken before accelerating downwards increases with temperature regardless of ratchet directionality, eluding again to the presence and influence of a greater vapor volume. However, here the contribution of the vapor layer is less clear. An AR of 11.4 shows no noticeable trend in observed decelerations after impact and ensuing accelerations; however, times to begin accelerating increase with temperature as observed with an AR of 2.2. Again, the

influence of the vapor layer is unclear. Ratchet directionality appears relevant when increasing the temperature of cylinders defined by an AR of 2.2. Cylinders initially heated to 350 °C show that downward-facing ratchets will decelerate more than upward-facing ratchets. This trend reverses as temperature increases, with upward-facing ratchets presenting greater decelerating forces than downward-facing ratchets. For cylinders initially heated to 450 °C, upward-facing ratchets result in 0.11 m/s² more deceleration than downward-facing ratchets, and the difference increases to 0.14 m/s² for cylinders initially heated to 550 °C. Preliminarily, we propose that traditional viscous drag [7] behavior contributes to the differences seen within the transient state.

At the immediate stage after surface impact, we suggest that the vapor layer is thin, regardless of initial temperature, and remains so for as long the vapor has a direct route of escape into the atmosphere. For cylinders initially heated to 350 °C, upward-facing ratchets take 0.52 s longer than when ratchets face downward to begin descending; however, downward-facing ratchets take 0.11 s and 0.14 s longer to begin their descent when initially heated to 450 °C and 550 °C, respectively. The vapor flow is driven by buoyancy, and the ratchets fail to rectify that flow the hotter the cylinder is. Once accelerating, downward-facing ratchets show higher accelerations when initially heated to 350 °C and 450 °C with a difference of 0.06 m/s² and 0.09 m/s². When initially heated to 550 °C, we see no difference between downward and upward facing ratchets. These latter observations agree with our hypothesis that the vapor layer increases in thickness due to the suppression of vapor escape. Vapor escape is prevented by the bulk fluid that encapsulates the cylinders from above, and so we
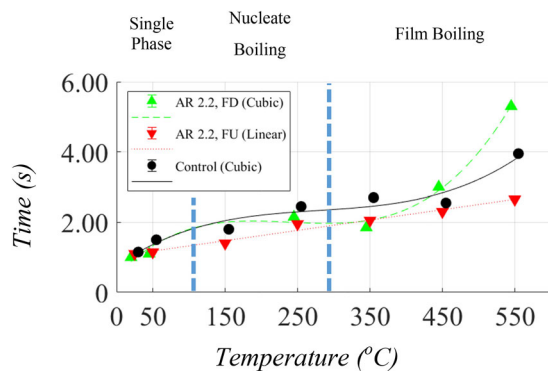

Figure 16. Time taken for smooth and ratcheted cylinders with aspect ratios of 2.2 to reach terminal velocity plotted against temperature. Vertical blue dashed lines are included as an approximation to characterize the preferential regime taking place during most of the fall and during terminal velocity.
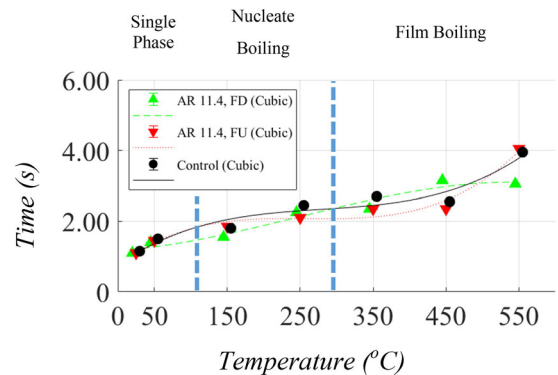

Figure 17. Time taken for smooth and ratcheted cylinders with aspect ratios of 11.4 to reach terminal velocity plotted against temperature. Vertical blue dashed lines are included as an approximation to characterize the preferential regime taking place during most of the fall and during terminal velocity.

expect the viscous drag force to decrease in magnitude as the proportion of vapor flow that gets rectified decreases.

Steady-state and terminal velocity

At the steady-state condition, we assume that the force of gravity is balanced by buoyancy forces associated with the cylinder body and the surrounding volume of vapor or entrained air, self-propelling viscous drag forces, form drag, and skin friction. Here, we assume a constant velocity and present the time to reach a steady state alongside the depth the forces became balanced.

Time

The time to reach terminal velocity, v_t (m/s), for the different temperatures studied for the control and 2.2FD, and 2.2FU is presented in Figure 16.

Control – Time to reach terminal velocity increases with temperature within a given boiling regime; however, we see a plateau or a negative relation during or even after the transition from one regime to another. In the single phase, the time taken to reach terminal velocity increases from 1.15 s to 1.50 s for SC-IH25 compared to SC-IH50. Similarly, within the nucleate boiling regime, the time to reach terminal velocity increases with temperature from 1.80 s for SC-IH150 to 2.45 s for SC-IH250. SC-IH350 takes 2.70 s to reach terminal velocity, compared to 2.55 s and 3.95 s for SC-IH450 and SC-IH550, respectively.

Aspect ratio 2.2 – A 2.2FD topology results in longer falling times within the single-phase regime when compared to a 2.2FU topology. Drag forces delay a 2.2FD cylinder's terminal velocity in comparison to a 2.2FU cylinder falling within the nucleate boiling regime. The transition between the nucleate and film boiling regimes increases vapor flow rectification. Once a vapor film has stabilized, 2.2FD ratchets result in more significant overall drag than both SC and 2.2FU topologies. A 2.2FD topology takes 1.00 s to reach terminal velocity within the single-phase compared to 1.10 s for a 2.2FU topology at isothermal conditions.

Furthermore, a 2.2FD-IH50 cylinder takes 1.10 s to reach terminal velocity compared to 1.15 s for a 2.2FU-IH50 cylinder. A 2.2FU-IH150 cylinder takes 1.40 s to reach terminal velocity. A cylinder initially heated to 250 °C provides the only direct comparison within the nucleate boiling regime, with 2.2FD-IH250 taking 2.15 s to reach terminal velocity compared to 2.2FU-IH250 at 1.95 s. Within the film boiling regime, a 2.2FD cylinder takes 1.85 s, 3.00 s, and 5.30 s for cylinders initially heated to 350 °C, 450 °C, and 550 °C, while 2.2FU cylinders take 2.05 s, 2.30 s, and 2.65 s, respectively.

Aspect Ratio 11.4 – The time to reach terminal velocity, v_t (m/s) for the different temperatures studied for the control and 11.4FD and 11.4FU is presented in Figure 17. There is little ratchet directional dependence within the single-phase regime. The nucleate boiling regime indicates no clear directional dependence due to instabilities. A plateau observed with an 11.4FD cylinder suggests the existence of a limit to the increase in form drag for objects falling beyond the Leidenfrost point [29]. An 11.4FD-IH25 cylinder and an 11.4FD-IH50 cylinder take 1.10 s and 1.40 s to reach terminal velocity. An 11.4FU-IH25 and an 11.4FU-IH50 cylinder take 1.10 s and 1.45 s to reach terminal velocity when falling within a single phase. The nucleate boiling regime presents an 11.4FD-
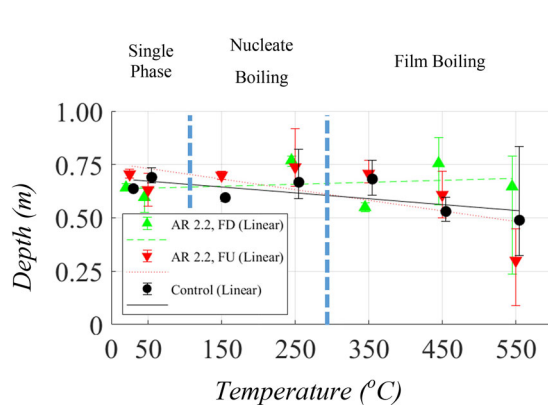

Figure 18. Depth at which smooth and ratcheted cylinders with aspect ratios of 2.2 reached their terminal velocity plotted against temperature. Vertical blue dashed lines are included as an approximation to characterize the preferential regime taking place during most of the fall and during terminal velocity.
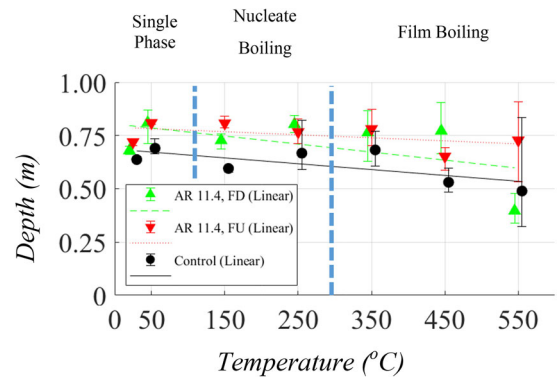

Figure 19. Depth at which smooth and ratcheted cylinders with aspect ratios of 11.4 reached their terminal velocity plotted against temperature. Vertical blue dashed lines are included as an approximation to characterize the preferential regime taking place during most of the fall and during terminal velocity.

IH150 cylinder to take 1.55 s while an 11.4FU-150 cylinder takes 1.85 s to reach terminal velocity. For cylinders initially heated to 250 °C, an 11.4FD topology presents 2.25 s, while an 11.4FU cylinder takes 2.10 s to plateau. Within film boiling, for cylinders initially heated to 350 °C, 450 °C, and 550 °C, an 11.4FD topology gives 2.35 s, 3.15 s, and 3.05 s, compared to an 11.4FU topology which gives 2.35 s, 2.35 s, and 4.05 s, respectively.

Depth

The depth at which terminal velocity, v_t (m/s), was reached for the different temperatures studied for the control and 2.2FD and 2.2FU is presented in Figure 18.

Control – Initially, heating a cylinder causes a cylinder falling within the single-phase regime to reach a deeper position before forces balance. Similarly, an increasing initial temperature within the nucleate boiling regime will force a cylinder deeper before reaching terminal velocity. This trend reverses within the film boiling regime, and the higher the initial temperature, the shallower the plateau depth. In the single-phase regime, an SC-IH25 and an SC-IH50 cylinder reach terminal velocity at 0.64 ± 0.01 m and 0.69 ± 0.04 m. The nucleate boiling regime presents the depths of an SC-IH150 and SC-IH250 cylinder to be 0.60 ± 0.02 m and 0.67 ± 0.11 m, respectively. In the presence of a vapor film, a smooth cylinder reaches its terminal velocity at depths of 0.68 ± 0.08 m, 0.53 ± 0.06 m, and 0.49 ± 0.25 m.

Aspect ratio 2.2 – In the single-phase regime, 2.2FD cylinders reach terminal velocities at shallower depths compared to 2.2FU topologies. Furthermore, the higher the initial temperature, the shallower the plateau. 2.2FD cylinders travel deeper than their 2.2FU
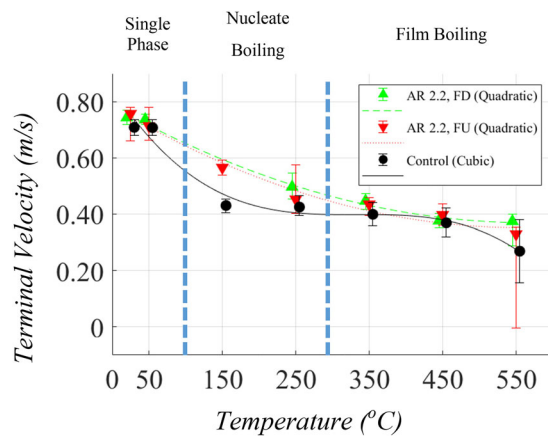
counterparts within the nucleate boiling regime, and we find that higher initial temperatures result in deeper observations. Initially, we see 2.2FU cylinders traveling deeper before forces balance within the film boiling regime compared to 2.2FD topologies; however, this trend reverses as vapor film thicknesses increase. For 2.2FU cylinders, the higher the initial temperature, the shallower the occurrence of terminal velocity, while 2.2FD cylinders do not present such a clear trend. 2.2FD-IH350 gives the shallowest reading, while 2.2FD-IH250 reaches the deepest depths before forces balance. 2.2FD-IH25 and 2.2FD-IH50 cylinders plateau at 0.64 ± 0.02 m and 0.60 ± 0.06 m within the single-phase regime. For 2.2FU-IH25 and 2.2FU-IH50, comparable depths are 0.70 ± 0.02 and 0.63 ± 0.08 m.

The nucleate boiling regime offer depths of 0.70 ± 0.02 m and 0.74 ± 0.14 m for 2.2FU-IH150 and 2.2FU-IH250 cylinders. 2.2FD-IH250 reaches a steady state at 0.77 ± 0.03 m. Within the film boiling regime, 2.2FD-IH350, 2.2FD-IH450, and 2.2FD-IH550 cylinders reach their respective terminal velocities at depths of 0.55 ± 0.02 m, 0.76 ± 0.16 m, and 0.65 ± 0.28 m. Comparable 2.2FU results were presented as 0.70 ± 0.05 m, 0.61 ± 0.11 m, and 0.30 ± 0.18 m.

Aspect Ratio 11.4 – The depth at which terminal velocity, v_t (m/s), was reached for the different temperatures studied for the control and 11.4FD and 11.4FU is presented in Figure 19. At isothermal conditions, we see that an 11.4FD topology results in shallower readings compared to 11.4FU cylinders; however, the ratchet design is less influential for cylinders initially heated to 50 °C. Both cylinders within
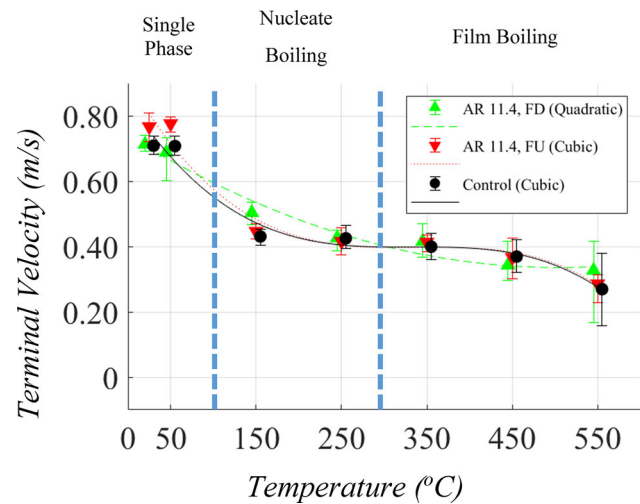

Figure 20. Terminal velocity for smooth and ratcheted cylinders with an aspect ratio of 2.2 plotted against temperature. Vertical blue dashed lines are included as an approximation to characterize the preferential regime taking place during most of the fall and during terminal velocity.

Figure 21. Terminal velocity for smooth and ratcheted cylinders with an aspect ratio of 11.4 plotted against temperature. Vertical blue dashed lines are included as an approximation to characterize the preferential regime taking place during most of the fall and during terminal velocity.

the single-phase regime fall to a deeper depth as the initial temperature increases.

This trend is again seen within the nucleate boiling regime with an 11.4FD topology; however, for 11.4FU cylinders, the higher the initial temperature, the lower the depth at which the terminal velocity will occur. The film boiling experiments present inconclusive results, where for an 11.4FU cylinder, we see an initial decrease in depth before the following increase. At the same time, there is a very slight initial increase for an 11.4FD topology before a significant decrease in the depth at which cylinders reach their terminal velocity.

Forces of an 11.4FD-IH25 cylinder balance at a depth of 0.68 ± 0.02 m. The same holds for 11.4FD-IH50, 11.4FU-IH25, 11.4FU-IH50 cylinders withcorresponding depths with the single-phase regime of 0.81 ± 0.08 m, 0.72 ± 0.02, and 0.80 ± 0.01 m. Within the nucleate boiling regime, we see depths of 0.73 ± 0.03 m, 0.80 ± 0.04, 0.81 ± 0.03 m, and 0.77 ± 0.06 m corresponding to 11.4FD-IH150, 11.4FD-IH250, 11.4FU-IH150, and 11.4FU-IH250. A vapor film influences the depths of 11.4FD $(0.76 \pm 0.12$ m, 0.77 ± 0.12 m, and 0.40 ± 0.07 m) and 11.4FU $(0.78 \pm 0.08$ m, 0.65 ± 0.06 m, and 0.73 ± 0.18 m) cylinders initially heated to 350 °C, 450 °C and 550 °C, respectively.

Terminal velocity

The terminal velocity, v_t (m/s), for the different temperatures studied using control, and 2.2FD and 2.2FU cylinders are presented in Figure 20.

Control – The terminal velocity is unaffected by a cylinder's temperature when falling within a single-phase and nucleate boiling regime; however, the terminal velocity is significantly lower in the latter regime. Once in the film boiling regime, the terminal velocity decreases in an almost quadratic fashion. The terminal velocities corresponding to the single-phase are 0.71 ± 0.03 m/s and 0.71 ± 0.03 m/s for an isothermal and a cylinder initially heated to 50 °C. Nucleate boiling reduces the terminal velocities to 0.43 ± 0.03 m/s for cylinders initially heated to 150 °C and 250 °C. Cylinders initially heated to 350 °C fall at 0.40 ± 0.04 m/s compared to 0.37 ± 0.05 m/s and 0.27 ± 0.11 m/s for cylinders initially heated to 450 °C and 550 °C.

Aspect ratio 2.2 – Unlike the control, a 2.2FU cylinder's velocity decreases almost linearly in the single-phase and through to the nucleate boiling regime. We see a marginal plateau as we transition into the film boiling regime, and then like with the control, an almost parabolic decline ensues. We see a minor decrease in velocity for a 2.2FD topology within the

single phase. Behavior within the nucleate boiling regime is mostly inconclusive; however, we see an initial decrease in terminal velocity in the film boiling regime followed by an increase between cylinder initially heated to 450 °C and 550 °C.

For the single-phase conditions, 2.2FD-IH25, 2.2FD-IH50, 2.2FU-IH25, and 2.2FU-IH50 cylinders fall at 0.71 ± 0.03 m/s⁻1, 0.69 ± 0.07 m/s, 0.77 ± 0.04, and 0.78 ± 0.02 m/s. Again, the nucleate boiling regime causes slower falling cylinders with 0.50 ± 0.03 m/s, 0.43 ± 0.03 m/s, 0.45 ± 0.02, and 0.42 ± 0.04 m/s corresponding to 2.2FD-IH150, 2.2FD-IH250, 2.2FU-IH150, and 2.2FU-IH250, respectively. 2.2FD-IH350, 2.2FD-IH450, and 2.2FD-IH550 fall at 0.42 ± 0.05 m/s, 0.34 ± 0.06, and 0.33 ± 0.12 m/s. 2.2FU cylinders present with 0.41 ± 0.03 m/s, 0.36 ± 0.06, and 0.29 ± 0.05 m/s, respectively. Considering 2.2FD cylinders in the single phase, an isothermal cylinder falls at 0.74 ± 0.03 m/s and a cylinder initially heated to 50 °C also falls at 0.74 ± 0.02 m/s. In the nucleate boiling regime, a 2.2FD-IH250 cylinder falls at 0.50 ± 0.05 m/s. 2.2FU-IH150 and 2.2FU-IH250 cylinders fall at 0.57 ± 0.03 m/s and 0.54 ± 0.09 m/s. Film boiling experiments include cylinders initially heated to 350 °C, 450 °C, and 550 °C, which for 2.2FD cylinders present 0.45 ± 0.03 m/s, 0.38 ± 0.03, and 0.37 ± 0.06 m/s. Comparable 2.2FU cylinders fall at 0.43 ± 0.03 m/s, 0.40 ± 0.04, and 0.33 ± 0.18 m/s.

Aspect Ratio 11.4 – The terminal velocity, v_t (m/s), is presented for the different temperatures studied for the control, and 2.2FD and 2.2FU are presented in Figure 21. The single-phase presents two opposing trends between an 11.4FD and an 11.4FU topology. An 11.4FD cylinder repeats trends seen above, with a slightly decreasing terminal velocity as temperatures increase, but the 11.4FU cylinder increases terminal velocity.

We see two decreasing parabolic slopes during the nucleate boiling regime, a steeper trend with an 11.4FD cylinder and a lesser slope with an 11.4FU cylinder. Beyond the Leidenfrost point, the 11.4FU cylinder follows the trajectory of the smooth cylinder by decreasing increasingly, while the 11.4FD cylinders appear to plateau as temperatures rise.

Force balance

Consider that cylinders are perfectly encapsulated in a vapor layer when in the film boiling regime. Consider that the vapor layer thickness, shape, and volume remain constant throughout the fall, in so far as one could assume perfect free-falling cylinders that are

Table 7. Quantification of the viscous friction, F_{VF}, force due the rectification of vapor flows within the vapor layer caused by the Leidenfrost effect.

Description	Time, s	F_R, mN	F_D, mN	F_{VF}, mN
11.4FU-IH350	2.35	5.4611	92.69	1.32
11.4FU-IH450	2.35	5.4611	93.10	1.74
11.4FU-IH550	4.05	1.8387	95.03	0.04
11.4FD-IH350	2.35	5.4611	92.69	1.32
11.4FD-IH550	3.05	3.2420	95.03	1.45
2.2FU-IH350	2.05	7.1764	92.60	2.96
2.2FU-IH450	2.30	5.7011	93.18	2.06
2.2FU-IH550	2.65	4.2946	95.81	3.28
2.2FD-IH450	3.00	3.3510	93.18	0.29
2.2FD-IH550	5.30	1.0736	95.81	0.06

The vapor volume is assumed equal for all cylinders. Therefore, the balance of gravity and buoyancy, $F_G - F_B$, is equal for all cylinders, quantified as 96.82 mN. The drag force, F_D, is calculated using the smooth cylinders. The resultant force was found using equation (7).

positioned parallel to the column. Imagine then that the rate of change of velocity is constant and that the trajectory follows an initial velocity of zero to the terminal velocity for a given cylinder. Imagine also that the distance traveled is equal to the depth measured and that the drag force is equal for all cylinders that fall with an equal terminal velocity. In such a scenario the mass of vapor is negligible compared to that of the cylinder, where equation (5) shows the mass of the vapor-cylinder combination.

$$m = \rho_c V \qquad (5)$$

Where m represents mass, V is the volume of the vapor-cylinder combination, ρ_c is the density of an aluminum cylinder.

Figure 17 shows that at initial temperatures $450\,^\circ\text{C}$ and $550\,^\circ\text{C}$, all cylinders (SC, 2.2FD, and 2.2FU) reach terminal velocity at the same depth within an acceptable margin of error. Similarly, Figure 19 shows that the margin of error around the measured terminal velocity is such that we may assume that terminal velocity is equal for all cylinders.

Consider the force balance around a smooth cylinder falling within the film boiling regime. Equation (6) shows the force balance for this scenario.

$$F_R = F_G - F_B - F_D \qquad (6)$$

Where F_D is the drag force, F_G is the gravitational force, F_B is the buoyancy force, and F_R is the overall resultant force. Using the assumptions outlined above, we can define the resultant force in terms of time and distance using equation (7).

$$F_R = m\left(\frac{2s}{t^2}\right) \qquad (7)$$

Where, s is the depth measured when an object reaches terminal velocity, and t is the time taken for a

cylinder to reach terminal velocity. We can also define the balance of gravitational and buoyancy forces using equation (8).

$$F_G - F_B = Vg(\rho_c - \rho_f) \qquad (8)$$

Where g is gravity and so using equations (6–8), we can then state the drag force for SC-IH350, SC-IH450, and SC-IH550 defined in equation (9).

$$F_{D,SC} = (F_{G,SC} - F_{B,SC}) - F_{R,SC} \qquad (9)$$

Drag within a submerged environment is a force associated with the shape of an object and the interactions at the interface of the liquid. In the case of film boiling, we assume a perfectly encapsulated cylinder where the interface with the liquid is equal for all cylinders. Equation (10) then assumes that the drag force calculated using a smooth cylinder is the same for the ratcheted cylinders regardless of topology.

$$F_{D,SC} = F_{D,RC} \qquad (10)$$

Here then, where error margins associated with depth and terminal velocity overlap, we can use the differences in recorded time to define the magnitude and direction of the viscous friction force. Equation (11) shows the force balance for ratcheted cylinders in the film boiling regime and how to quantity the viscous friction force, F_{VF}.

$$F_{VF,RC} = |(F_{G,RC} - F_{B,RC}) - F_{R,RC} - F_{D,SC}| \qquad (11)$$

For ratcheted cylinders where the error margins concerning depth and velocity do not overlap with those associated with the smooth cylinder, one cannot define the viscous friction force. Table 7 quantifies the viscous friction force for all the cylinders to which the assumptions described above apply. No overlap in error margins meant that 2.2FD-IH350 and 11.4FD-IH450 could not be assumed to fall at an equal depth to SC-IH350 and SC-IH450 respectively.

11.4FD-IH450 falls for longer than SC-IH450 but reaches terminal velocity at a greater depth. 2.2FD-IH350 falls for less time than SC-IH350 but reaches terminal velocity at a shallower depth. Both results are intuitive with a traditional understanding of submerged free-fall, leaving no conclusive evidence of self-propulsion in these cases.

Ratchet directionality

Ratchet directionality may be investigated by comparing ratcheted cylinders with equal aspect ratios falling at the same conditions. Again, if error margins in depth and terminal velocity allow, one can compare temporal measurements to gain an insight to the

behavior of the viscous friction force. For all temperatures, error margins in the measured terminal velocity allow for direct comparison in all cases.

Only IH450 and IH550 present measurements where 2.2FD and 2.2FU may be assumed to have reached their terminal velocity at the same depth. For 11.4FD and 11.4FU, the depths at which terminal velocity was reached may be assumed equal for IH350 and IH450.

If we consider only these four experiments and using Figures 16 and 17, we can view the ratchet directional dependance with cylinders that fall within the film boiling regime. In three of four cases, an FD topology yields a cylinder that takes longer to reach terminal velocity. The fourth case yields a result of equivalence. We also see that the time difference between FD and FU topologies increases with temperature, suggesting a stronger force of viscous friction as temperature increases.

Conclusions

Experiments investigating the free-fall of five cylinders boiling beyond the Leidenfrost point with varying topologies show ratchet directional dependency. Hollow aluminum cylinders with lengths of 40 mm, diameters of 10 mm, and hollows 50% V/V present with a sustained vapor film if heated to 350 °C and beyond. Inconclusive evidence suggests the existence of submerged self-propulsion when comparing ratcheted cylinders. Vapor produced from boiling dominates a free-fall, ultimately reducing the terminal velocity regardless of cylinder topology. Increasing the vapor film around ratcheted cylinders increases the likelihood of observing self-propulsion within a submerged environment. The longer a cylinder takes to reach terminal velocity, the cooler it is relative to its initial temperature at the measurement point, thus the thinner the vapor layer. A thinner vapor layer should decrease buoyancy forces and increase the drag coefficient and viscous friction forces.

Barriers to determining vapor volume and drag coefficients of superheated free-falling objects limit the application of the data presented herein. Furthermore, experimental techniques to monitor cylinder temperature during free-fall remains challenging. However, significant experimental results and good experimental error data in velocity, depth, and time could allow for the development of theoretical tools to predict and model the behavior of heated and superheated objects that free-fall in submerged environments.

We develop a theoretical approach to identify the viscous friction force for cylinders that fall within the film boiling regime. We compare ratcheted cylinders with opposing ratchet directionality that may be assumed to reach terminal velocity at an equal depth. Our results present an interesting situation whereby ratcheted cylinders with an FD topology take longer to reach their terminal velocity compared with their FU counterparts. This observation implies that when ratchet structures face downward, the viscous friction force opposes free-fall, while upward facing ratchets aids free-fall. One can point toward observations of ratchet self-propulsion because the self-propelling force for FU cylinders would be in the direction of the fall.

Additionally, we develop a theoretical approach to quantify the viscous friction force for cylinders falling in the film boiling regime. We compare ratcheted cylinders with a smooth control, where the control cylinder and a given ratcheted cylinder may be assumed to reach an equal terminal velocity at an equal depth. We use the calculated drag force from the smooth control to close the force balance in the case of a ratcheted cylinder. With this approach we define the viscous friction force within the film boiling regime to be between $0.04 - 3.28$ mN. The direction of the ratchets play an important role in so far as an upward facing ratchet yields stronger viscous friction forces than their downward facing counterparts. The role of ratchet aspect ratio also appears important. When ratchets face upwards, a smaller aspect ratio yields a stronger viscous friction force. Comparatively, when ratchet face downwards the larger aspect ratio yields the stronger viscous friction force. Cylinder 2.2FU yields the strongest viscous friction force consistently across all tested initial temperatures.

The theoretical force balances would suggest the presence of self-propelling viscous drag forces for ratcheted cylinders falling within the film boiling regime. Terminal velocity and the depth at which terminal velocity occurs appears to be mostly unaffected by the addition of a vapor layer when comparing ratcheted cylinders to smooth cylinders; however, when viewing the time taken to reach terminal velocity, we are able to identify and quantify the effect of the viscous friction force – which either extends or shortens the time taken to reach terminal velocity. Temporal changes depend on the direction that the ratchet structures face; however, without a definition of drag coefficients and reasonable estimates of the surrounding vapor volume, results herein remain inconclusive due to the significant uncertainty arising from falling cylinders while boiling in the Leidenfrost regime.

Acknowledgments

Notes on contributors

Adrian Jonas read Chemical Engineering at the University of Edinburgh, where he completed the integrated master's program in 2020. He developed a passion for experimental research during his master's year, where he worked alongside Dr. Anthony Buchoux and Prof. Khellil Sefiane to develop a micro heat engine that uses the Leidenfrost effect for energy production. He joined Prof. Sefiane's research group in 2020, where he is currently studying toward a PhD at the University of Edinburgh.

Daniel Orejon holds a 5-year bachelor's degree in Environmental and Industrial Chemical Engineering from the University of Seville (Spain), including one year as an undergraduate research assistant. After graduating, he spent a year as a graduate research assistant at the Institute for Energy Systems at the University of Edinburgh. After that, he completed his PhD on the fundamentals of evaporation phase-change at the droplet scale, both during free evaporation and under external forces applied in 2013. Shortly after, he joined the International Institute for Carbon-Neutral Energy Research (WPI-I2CNER) at Kyushu University in Japan as a Post-Doctoral Research Associate. He shifted his research efforts toward condensation phase-change while continuing his research interests and collaborations on droplet evaporation. In 2016, he became WPI-I2CNER Assistant Professor at Kyushu University (Japan), and two years later, he joined the University of Edinburgh as a Lecturer in Chemical Engineering at the Institute for Multiscale Thermofluids; where he additionally serves as School Postgraduate Progression Committee Representative for the Institute for Multiscale Thermofluids and as Teaching Laboratory Manager for the Chemical Engineering Discipline. In addition, he has been appointed WPI-I2CNER Visiting Associate Professor since April 2019, he served as Associate Editor for the International Journal of Heat and Mass Transfer since January 2021, and he has been a Fellow of the Higher Education Fellow since April 2021.

Khellil Sefiane, FRSC, FInstP, FJSPS, is a Professor of Thermophysical Engineering at the University of Edinburgh, Assoc. Editor of Int. J. Heat and Mass Transfer, and RAEng ExxonMobil Fellow with more than 250 journal papers, and expert in novel experimental techniques for heat and mass transfer, phase change, moving contact lines, and flow regime transitions in mixtures. He has received the IoP Printing & Graphics Science Group Prize (2009) for his "Fundamental studies on droplet evaporation" as well as the Royal Academy of Engineering Global Research Award and elected the UK representative on the EUROTHERM Committee, member of the Scientific Council of the Int. Center for Heat and Mass Transfer. He has been an associate editor for the ASME Journal of Heat Transfer and the International Journal of Multiphase Flows.

ORCID

Adrian Jonas 🆔 http://orcid.org/0000-0003-2668-2620
Daniel Orejon 🆔 http://orcid.org/0000-0003-1037-5036
Khellil Sefiane 🆔 http://orcid.org/0000-0003-3300-0210

References

[1]   J. G. Leidenfrost, "On the fixation of water in diverse fire," *Int. J. Heat Mass Transf.*, vol. 9, no. 11, pp. 1153–1166, 1966. DOI: 10.1016/0017-9310(66)90111-6.

[2]   J. T. Ok, J. Choi, E. Brown and S. Park, "Effect of different fluids on rectified motion of Leidenfrost droplets on micro/sub-micron ratchets," *Microelectron Eng.*, vol. 158, pp. 130–134, 2016. Jun. DOI: 10.1016/j.mee.2016.04.018.

[3]   S. D. Janssens, S. Koizumi and E. Fried, "Behavior of self-propelled acetone droplets in a Leidenfrost state on liquid substrates," *Phys. Fluids*, vol. 29, no. 3, pp. 032103 Mar. 2017. DOI: 10.1063/1.4977442.

[4]   G. Lagubeau, M. L. Merrer, C. Clanet and D. Quéré, "Leidenfrost on a ratchet," *Nat. Phys.*, vol. 7, no. 5, pp. 395–398, 2011. DOI: 10.1038/nphys1925.

[5]   S. Diniega, et al., "A new dry hypothesis for the formation of martian linear gullies," *Icarus*, vol. 225, no. 1, pp. 526–537, 2013. DOI: 10.1016/j.icarus.2013.04.006.

[6]   A. L. Biance, C. Clanet and D. Quéré, "Leidenfrost drops," *Phys. Fluids*, vol. 15, no. 6, pp. 1632–1637, 2003. DOI: 10.1063/1.1572161.

[7]   H. Linke, et al., "Self-propelled leidenfrost droplets," *Phys. Rev. Lett.*, vol. 96, no. 15, pp. 2–5, 2006. DOI: 10.1103/PhysRevLett.96.154502.

[8]   A. Bouillant, et al., "Leidenfrost wheels," *Nat. Phys.*, vol. 14, no. 12, pp. 1188–1192, 2018. DOI: 10.1038/s41567-018-0275-9.

[9]   G. Dupeux, et al., "Viscous mechanism for Leidenfrost propulsion on a ratchet," *EPL*, vol. 96, no. 5, pp. 58001 Dec. 2011. DOI: 10.1209/0295-5075/96/58001.

[10] M. Mrinal, X. Wang and C. Luo, "Self-rotation-induced propulsion of a leidenfrost drop on a ratchet," *Langmuir*, vol. 33, no. 25, pp. 6307–6313, 2017. DOI: 10.1021/acs.langmuir.7b01420.

[11] A. Würger, "Leidenfrost gas ratchets driven by thermal creep," *Phys. Rev. Lett.*, vol. 107, no. 16, pp. 164502–4, 2011. DOI: 10.1103/PhysRevLett.107.164502.

[12] D. Soto, G. Lagubeau, C. Clanet and D. Quéré, "Surfing on a herringbone," *Phys. Rev. Fluids*, vol. 1, no. 1, pp. 1–10, 2016. DOI: 10.1103/PhysRevFluids.1.013902.

[13] P. Agrawal, et al., "Leidenfrost heat engine: Sustained rotation of levitating rotors on turbine-inspired substrates," *Appl. Energy*, vol. 240, pp. 399–408, 2019. Feb. DOI: 10.1016/j.apenergy.2019.02.034.

[14] T. R. Cousins, R. E. Goldstein, J. W. Jaworski and A. I. Pesci, "A ratchet trap for Leidenfrost drops," *J. Fluid Mech.*, vol. 696, pp. 215–227, 2012. Apr. DOI: 10.1017/jfm.2012.27.

[15] G. Dupeux, et al., "Self-propelling uneven Leidenfrost solids," *Phys. Fluids*, vol. 25, no. 5, pp. 051704–7, 2013. DOI: 10.1063/1.4807007.

[16] R. L. Agapov, et al., "Length scale of Leidenfrost ratchet switches droplet directionality," *Nanoscale*, vol. 6, no. 15, pp. 9293–9299, 2014. DOI: 10.1039/c4nr02362e.

[17] G. Duursma, R. Kennedy, K. Sefiane and Y. Yu, "Leidenfrost droplets on microstructured surfaces," *Heat Transf. Eng.*, vol. 37, no. 13–14, pp. 1190–1200, 2016. DOI: 10.1080/01457632.2015.1112610.

[18] A. Hashmi, et al., "Leidenfrost levitation: beyond droplets," *Sci. Rep.*, vol. 2, pp. 797 Nov. 2012. DOI: 10.1038/srep00797.

[19] M. Shi, et al., "Self-propelled hovercraft based on cold Leidenfrost phenomenon," *Sci. Rep.*, vol. 6, pp. 28574 Jun. 2016. DOI: 10.1038/srep28574.

[20] G. G. Wells, R. Ledesma-Aguilar, G. McHale and K. Sefiane, "A sublimation heat engine," *Nat. Commun.*, vol. 6, no. 1, pp. 7 Mar. 2015. DOI: 10.1038/ncomms7390.

[21] E. Kawakami and R. E. A. Arndt, "Investigation of the behavior of ventilated supercavities," *J. Fluids Eng.*, vol. 133, no. 9, pp. 091305, Sep. 2011. DOI: 10.1115/1.4004911.

[22] J. H. Spurk, "On the gas loss from ventilated supercavities," *Acta Mech.*, vol. 155, no. 3–4, pp. 125–135, 2002. DOI: 10.1007/BF01176238.

[23] E. L. Amromin, "Challenging problems on ventilated cavitation and paths to their computational solutions," *J. Mar. Sci. Appl.*, vol. 18, no. 3, pp. 260–270, 2019. DOI: 10.1007/s11804-019-00100.

[24] J. Wang, B. Wang and D. Chen, "Underwater drag reduction by gas," *Friction*, vol. 2, no. 4, pp. 295–309, 2014. DOI: 10.1007/s40544-014-0070-2.

[25] S. Ashley, "Warp drive underwater," *Sci. Am.*, vol. 284, no. 5, pp. 70–79, 2001. DOI: 10.1038/scientificamerican0501-70.

[26] I. U. Vakarelski, J. O. Marston, D. Y. C. Chan and S. T. Thoroddsen, "Drag reduction by leidenfrost vapor layers," *Phys. Rev. Lett.*, vol. 106, no. 21, pp. 214501–6, 2011. DOI: 10.1103/PhysRevLett.106.214501.

[27] K. H. Yeo, T. Zhou and K. C. Leong, "Experimental study of passive heat transfer enhancement in a drag-reducing flow," *Heat Transf. Eng.*, vol. 28, no. 1, pp. 9–18, 2007. DOI: 10.1080/01457630600985501.

[28] P. C. Chu, A. Gilles and C. Fan, "Experiment of falling cylinder through the water column," *Exp. Therm. Fluid Sci.*, vol. 29, no. 5, pp. 555–568, 2005. DOI: 10.1016/j.expthermflusci.2004.08.001.

[29] Q. S. Liu, K. Fukuda and M. Shiotsu, "Forced convection film boiling heat transfer over a vertical cylinder," *Heat Transf. Eng.*, vol. 32, no. 11–12, pp. 996–1002, 2011. DOI: 10.1080/01457632.2011.556469.